Chemical Science

ROYAL SOCIETY OF CHEMISTRY

REVIEW

View Article Online
View Journal | View Issue

Cite this: *Chem. Sci.*, 2025, **16**, 11711

Dual-metal synergistic catalysis for promoting electrocatalytic CO_2 reduction

Peng-Yu Shi, † Yan Yan, † Si-Yuan Yang, Jing-Jing Hao, Mei Wang * and Tong-Bu Lu *

The increasing emphasis on carbon neutrality has driven significant research into the electrochemical CO_2 reduction reaction (CO_2RR), aiming to convert CO_2 into value-added chemicals and fuels. Dual-metal catalysts, known for their synergistic effects, have garnered considerable attention due to their enhanced electrocatalytic performance for the CO_2RR by providing more active sites and optimizing intermediate interactions. Herein, this review will comprehensively explore how the synergistic effect between the two metal centers embedded within atomic and nanoparticle dual-metal catalysts facilitates the electrocatalytic CO_2RR, elucidating the structure–activity correlations. Recent significant progress of dual-metal catalysts with synergistic effects for promoting electrocatalytic CO_2 reduction will be summarized. Moreover, we will explore the design strategies of dual-metal catalysts and examine the influence of different types of metal active centers in the catalysts on the reaction pathway of the electrocatalytic CO_2RR, aiming to uncover profound insights for catalyst optimization and deepen mechanistic understanding of the catalytic process. Finally, the review identifies current research gaps and outlines future directions, emphasizing the need for innovative techniques to enhance catalytic stability and achieve multi-carbon products from the CO_2RR using dual-metal catalysts with synergistic effects. This topic could inspire extensive interest to further accelerate and explore the innovations of catalysts in energy conversion.

Received 1st May 2025
Accepted 4th June 2025

DOI: 10.1039/d5sc03193a

rsc.li/chemical-science

1 Introduction

The combustion of fossil fuels leads to substantial emissions of carbon dioxide and other greenhouse gases, exacerbating global warming and posing a grave threat to human survival and sustainable development.[1–6] Consequently, achieving carbon neutrality and mitigating temperature rise has garnered global consensus.[7–11] The conversion of CO_2 into high-value-added chemicals and fuels offers a promising pathway to close the artificial carbon cycle and address the environmental challenges caused by excessive CO_2 emissions.[12–16]

In CO_2, the carbon atom forms two strong C=O double bonds, each comprising a sigma (σ) and a pi (π) bond, ensuring its high chemical stability. This results in significant thermodynamic and kinetic barriers for the activation of CO_2, making its conversion pathways both critical and challenging.[17–20] Hence, developing effective methodologies and efficient catalysts holds great significance in advancing the carbon dioxide reduction reaction (CO_2RR). Various chemical methods have been utilized for CO_2 reduction, including electrocatalysis, thermal catalysis, photocatalysis, and bioconversion.[21–26] Electrocatalytic (CO_2RR) technology offers advantages such as simple equipment requirements, high environmental compatibility, and potential integration with intermittent or renewable electricity sources, making it a promising strategy for efficient CO_2 conversion.[27–29]

To date, significant advancements have been made in the field of the electrocatalytic CO_2RR. Various catalyst systems, ranging from nanomaterial catalysts to atomic catalysts, have been meticulously developed to tackle this complex process.[30–34] However, the intricacies of the multi-electron and multi-proton transfer reactions involved in the CO_2RR have posed numerous challenges, such as low efficiency, sluggish reaction rates and insufficient stability.[35–37] Among all types of catalysts, dual-metal catalysts have garnered particular attention. The modulation of CO_2RR catalysts with different active sites plays a vital role in solving the existing critical issues.[38] By introducing dual metal active sites into the catalysts, the electronic and geometric properties of the catalysts can be manipulated.[1,9,37,39] Crucially, this approach enables the realization of synergistic catalytic effects. For instance, such synergistic effects can be achieved wherein one metal site facilitates CO_2 activation while another one provides H^+ ions for CO_2 protonation.[40] Thereby, the synergistic effects between different active centres can lead to the optimization of the adsorption and activation of

School of Materials Science and Engineering, Institute for New Energy Materials & Low Carbon Technologies, Tianjin University of Technology, Tianjin 300384, China. E-mail: meiwang@email.tjut.edu.cn; lutongbu@tjut.edu.cn

† These authors contributed equally to this work.

reactants, transition state stabilization, and the desorption of products, as well as the refinement of the catalytic pathway for optimal performance for CO_2 reduction. The dual-metal catalysts can be broadly classified into two types: dual-atom metal catalysts and dual-metal nanomaterial catalysts.[1,9,41,42] Dual-atom catalysts can further be subdivided into homonuclear and heteronuclear dual-atom catalysts. Compared to single-atom catalysts, dual-atom catalysts offer much more advantages such as higher metal loading, more active sites, and more flexible adjustability for the CO_2RR.[43,44] By tuning the composition and arrangement of the two metal atoms in dual-atom catalysts, enhanced catalytic efficiency can be achieved compared to single-atom catalysts for the CO_2RR.[45,46] The synergistic effect between the two metal atoms can decrease the activation barriers for CO_2, directing the reaction pathway towards high selectivity. For example, Lu *et al.* reported an asymmetric TeN_2–CuN_3 catalyst with a synergistic mechanism: Te activates CO_2, while Cu aids H_2O dissociation, which significantly reduces the energy barrier and improves proton transfer kinetics for CO_2-to-CO reduction.[40] Dual-metal nanomaterial catalysts constitute another crucial class of catalysts for the electrochemical CO_2RR, experiencing notable advancements.[31] The copper metal exhibits weak hydrogen adsorption but moderate CO adsorption, effectively suppressing the hydrogen evolution (HER) and uniquely facilitating efficient production of multi-carbon products in CO_2 electroreduction.[47] Therefore, copper-based dual-metal nanomaterial catalysts stand out due to their distinct advantages in the electrocatalytic CO_2RR, demonstrating remarkable potential in facilitating the production of high-value C_{2+} products. For instance, Wang *et al.* constructed Ag–Cu dual sites in Ag-doped Cu_3N NC (Cu_3N–Ag NC), where CO is produced on Ag sites, and asymmetric C–C coupling to COCHO is promoted on Cu sites, leading to a marked increase in Faraday efficiency (FE) for C_2H_4 production compared to that of pure Cu_3N NC, which highlights the crucial role of the synergistic effects between the dual-metal Ag and Cu in the formation of multicarbon products.[48] There have been many reviews on electrocatalytic CO_2 reduction. Nevertheless, to date, there has been no review devoted to the impact of the synergistic effect of dual-active sites in the catalysts on the reaction pathway for the CO_2RR, which is of great significance in this area.

In this review, our primary goal is to offer a thorough examination of how dual-metal systems leverage their synergistic effects to optimize both electronic and geometric structures. Concurrently, these optimizations serve to enhance the functionality of dual-active sites, thereby achieving superior electrocatalytic performance towards the CO_2RR. First, we will delve into uncovering the design principles underlying dual-metal systems for the CO_2RR, with a primary focus on two key aspects: the precise modulation of the electronic structure and the control of the geometric configuration. In terms of electronic structure regulation, we will scrutinize three primary approaches such as chemical state, vacancy, and coordination environment modifications. Regarding geometric structure control, we will focus on several key parameters such as crystal facet, nanoparticle size, and morphology adjustments.

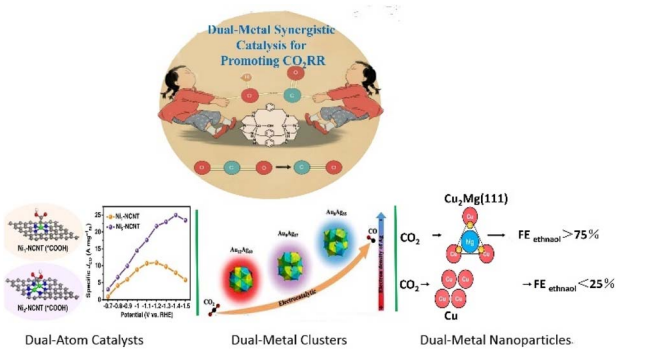

Scheme 1 Different types of dual-metal catalysts with synergistic effects for promoting electrocatalytic CO_2 reduction. Reproduced with permission.[124] Copyright 2023, Elsevier. Reproduced with permission.[96] Copyright 2023, Wiley-VCH Verlag. Reproduced with permission.[89] Copyright 2024, John Wiley and Sons Ltd.

Furthermore, we will systematically probe the way varying dual-metal active sites embedded within atomic (notably dual-atom catalysts, DACs) and nanoparticle catalysts affect CO_2RR catalytic performance, elucidating the pivotal role of synergistic effects in the fundamental reaction mechanisms. Specifically, we will investigate the synergistic dynamics within homonuclear and heteronuclear DACs systems. Additionally, an in-depth analysis will be conducted on nanomaterial catalysts that pair copper with main-group elements, non-precious metals, precious metals, and lanthanides, to elucidate their effects on catalytic mechanisms and overall efficiency in the CO_2RR. Finally, we identify the prevalent challenges and promising directions for the ongoing advancement of dual-metal catalysts, with the goal of enhancing electrocatalytic efficiency and stability for the production of multi-carbon compounds through the CO_2RR. This review will provide profound and insightful perspectives, thereby facilitating the rapid acceleration and in-depth exploration of innovations in dual-metal catalysts within the domain of energy conversion (Scheme 1).

2 Design principles of dual-metal catalysts with synergistic effects for the electrocatalytic CO_2RR

A vast array of design approaches has been meticulously investigated to enhance the electrocatalytic performance for the CO_2RR. The key design principles for dual-metal catalysts in the electrocatalytic CO_2RR involve electronic and geometric aspects, as these factors critically govern the formation of key intermediates, the pathway of C–C coupling, and the ability to suppress hydrogen evolution.[49] The electronic structure dictates the intrinsic catalytic properties by modulating the binding energy of reaction intermediates and steering the reaction pathway, while the geometric structure controls the physical arrangement of active sites, influencing reactant accessibility, mass transport, and the exposure of specific catalytic facets. By optimizing both of these aspects, dual-metal catalysts can

achieve enhanced efficiency and selectivity for converting CO_2 into valuable products. Therefore, prioritizing electronic and geometric structure regulation is essential for designing advanced catalysts that maximize performance and contribute to sustainable CO_2 utilization.[50]

2.1 Electronic structure regulation

Electronic structure regulation is a critical aspect of dual-metal catalyst design. By adjusting the chemical state of the metals, the valence state of the active sites can be stabilized or altered, which in turn influences their catalytic activity for the electrocatalytic CO_2RR.[51] Additionally, the incorporation of dual-metal catalysts can lead to the formation of vacancies or defects within the catalyst structure, which can highly tune the electronic structure of the catalyst.[52,53] Furthermore, coordination environment regulation can alter the local electronic sphere of metal active sites with synergistic interactions between the two metals, enhancing catalytic performance by tuning the energy levels of key intermediates during the CO_2RR process.[54]

2.1.1 Chemical state regulation. The valence state of the active sites is the most critical factor determining the catalytic efficiency of the catalyst for the electrocatalytic CO_2RR. By precisely regulating the chemical states, the reaction way can be steered towards the production of desired compounds, while minimizing the formation of byproducts, which is crucial for enhancing the efficiency of the CO_2RR.[55,56] For instance, previous studies have demonstrated that the Cu^+/Cu^0 mixed state plays a critical role in CO_2 electroreduction to multicarbon (C_{2+}) *via* reducing the kinetic barrier to C–C coupling.[57]

Dual-metal catalysts can leverage the tight interactions between two distinct metals to stabilize and/or modulate the chemical state of active sites. The electron density around the active sites can be modulated by the synergistic interaction between the two metals. Fine-tuning the valence states in dual-metal catalysts can lead to optimal adsorption and activation of CO_2 molecules, as well as the stabilization of key intermediates, thereby influencing its catalytic activity and product efficiency for the electrocatalytic CO_2RR.[58]

Many non-noble transition metals, such as Fe, Co, Ni, and Zn are used to as the second metal to stabilize the oxidation state of active metal sites, leveraging the synergistic catalytic effect of the two metals to enhance the performance of the electrocatalytic CO_2RR.[59–61] For example, Ma and Zhang's group reported that incorporating Ni into CuO nanosheets can stabilize the chemical state of Cu, meanwhile reinforcing the connections between Cu atoms located on the surface and those beneath the surface, resulting in a sustained FE_{C2+} and improved stability for the electrocatalytic CO_2RR compared to pure CuO nanosheets (Fig. 1a).[62] Choi *et al.* demonstrated that incorporating Zn into Cu_2O achieves two significant effects: it can stabilize Cu in a lower valence state (Cu^0), which is more active for CO_2 reduction; and it can lower the energy barrier for the OHC–CHO C–C coupling pathway, thereby promoting the formation of C_2H_4. These beneficial effects can be attributed to the charge transfer from Zn to Cu, which reduces Cu^+ to a lower and stable valence state and facilitates a more favorable reduction reaction at the Cu site (Fig. 1b).[56] Therefore, the combination of a second metal with the copper based catalyst can stabilize the valence state of the active site, leading to improve catalytic performance for the CO_2RR due to the synergistic effect.

In addition to maintaining the constant chemical state of the active sites, the second metal can also effectively regulate the chemical state of the active metal centers. Many noble metals or main group metals are used to modulate the oxidation state of the metal active centers. Kim *et al.* underscored the pivotal role of modulating the oxidation state by decorating copper (Cu) nanoparticles with iridium (Ir), leading to the charge transfer from Cu to Ir, which indicates that the oxidation state of Cu in the CuIr alloy is higher than that in Cu nanoparticles. By exploiting the robust affinity of Ir for oxygen, the electronic configuration of Cu is effectively modulated, thereby stabilizing oxygen-bound intermediates like CH_3CHO* and CH_3CH_2O* during the CO_2RR that are otherwise unstable on bare Cu catalysts. This valence state adjustment strategy markedly boosted the FE to 14.8% for reducing CO_2 to *tert*-butanol (*t*-BuOH), which represents a substantial improvement compared to that of pure Cu catalysts (Fig. 1c).[63] Loh's group constructed a $Cu/CaCO_3$ catalyst for the CO_2RR by integrating Cu nanoclusters with $CaCO_3$, in which the metal Ca can regulate the formation of dynamically stable $Cu^0/Cu^{\delta+}$ pair sites and maintain the $Cu^{\delta+}$ valence state. Consequently, the synergistic effect of the dual metal Cu and Ca can enhance adsorption capacity of CO_2 intermediate *CO and lower the C–C coupling energy barriers, achieving a remarkable FE of 83.7% for C_{2+} at a partial current density of 393 mA cm^{-2} (Fig. 1d).[64] The strategy of introducing a second metal to stabilize or modulate the valence state of catalytic centers is of great significance in designing and synthesizing highly efficient dual-metal catalysts. This approach can optimize intermediate binding, lower energy barriers and significantly enhance the electrocatalytic performance for the CO_2RR.

2.1.2 Vacancy regulation. Considerable progress has been made in developing dual-metal catalysts with enhanced efficiency through vacancy engineering, aimed at converting CO_2 into valuable chemicals. The vacancies within dual-metal catalysts have the ability to tune the electronic structure of the catalyst. The presence of vacancies can regulate the electronic cloud distribution around the metal atoms, and also create localized regions of high electron density leading to changes in energy levels and bonding properties. Specifically, these electron-rich sites are particularly well-suited for interacting with CO_2. Meanwhile, by serving as electron donors, the vacancy sites aid in weakening the double bonds in CO_2 and facilitate the formation of intermediate species, enhancing the overall electrocatalytic CO_2RR process.[65]

Of particular note are cationic vacancies, which have unique electronic structures and orbital distributions, and can greatly affect the properties of the metal catalysts for CO_2 reduction.[66–70] For instance, Sun *et al.* reported that introducing Sn dopants into a copper catalyst could modify the lattice structure of CuO, giving rise to the formation of oxygen vacancies, which have a significant impact on the surface electron distribution of the

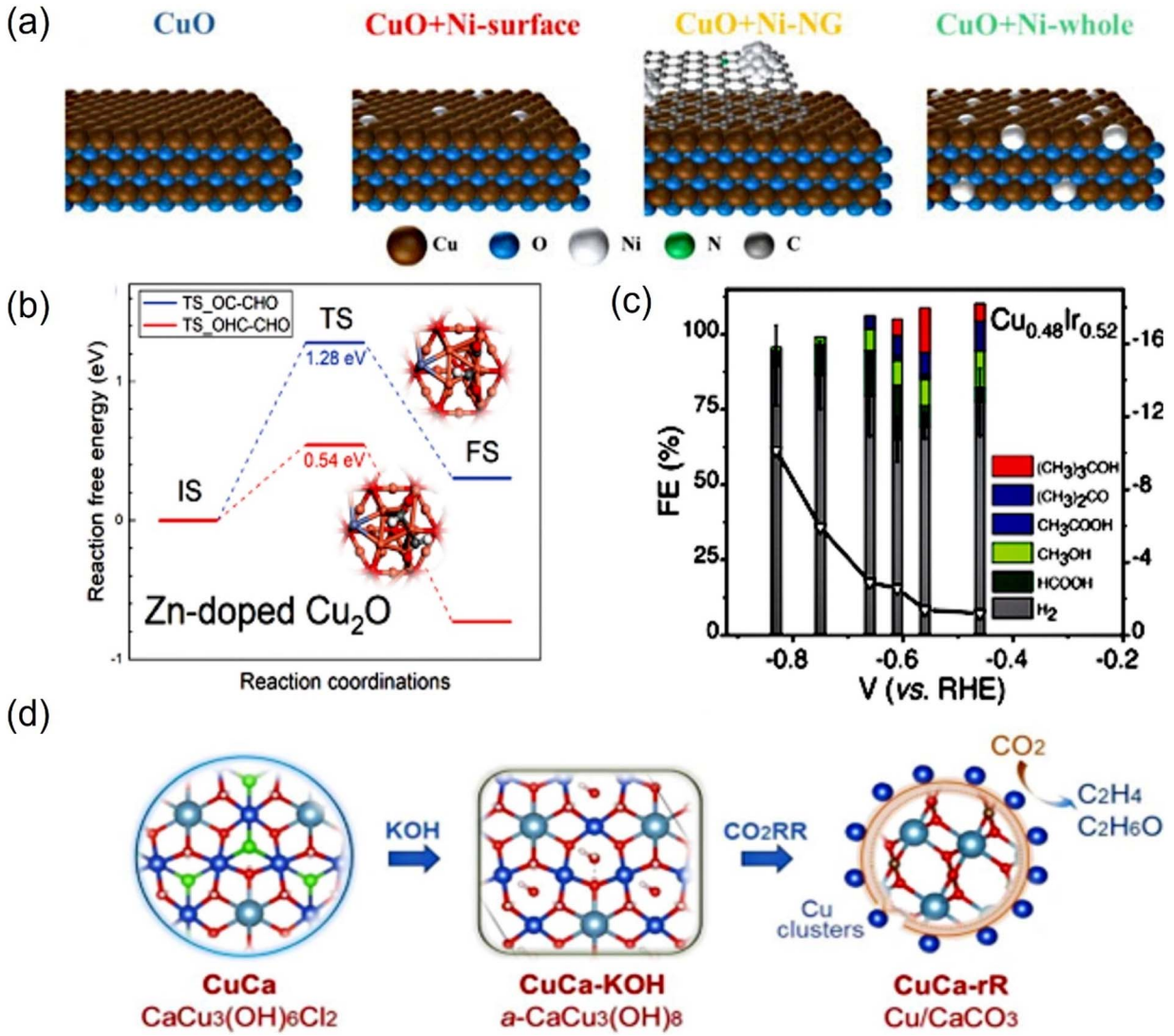

Fig. 1 (a) Different Ni-incorporated Cu catalysts. (b) Activation barrier diagram of C–C coupling on Zn-doped Cu_2O. (c) Potential-dependent faradaic efficiencies (FEs) for CO_2RR products and total current densities obtained by using $Cu_{0.48}Ir_{0.52}$. (d) Scheme of the reconstruction process to obtain Cu/$CaCO_3$. (a) Reproduced with permission.[62] Copyright 2025, Elsevier. (b) Reproduced with permission.[56] Copyright 2023, Wiley. (c) Reproduced with permission.[63] Copyright, 2023, Wiley. (d) Reproduced with permission.[64] Copyright 2025, John Wiley and Sons Ltd.

CuO nanosheets. DFT calculations confirmed that the synergistic effect of oxygen vacancies and the metals can strengthen CO_2 adsorption and reduce the energy barrier for the formation of intermediate species such as *COOH and *CO during the electroreduction process, leading to a substantial enhancement in the efficiency for electrocatalytic CO_2 reduction to CO (Fig. 2a).[71] Similarly, He, Xu, *et al.* constructed a series of dual-metal Cu/Ce catalysts with different concentrations of oxygen vacancies, in which the oxygen vacancies could alter the electronic microenvironment of the catalyst, leading to the introduction of uncoordinated metal site Cu^+ active centers. This revealed that the high concentration of oxygen vacancies in the dual-metal catalyst is crucial for facilitating the adsorption of *COOH and *CO intermediates, resulting in the efficient production of CH_4 with a FE of 70.03% and a TOF of 9946.7 h^{-1} (Fig. 2b).[70]

In addition to tuning the electronic structure of the catalyst, these vacancies in dual-metal catalysts can also act as active sites for the adsorption and conversion of CO_2. Xiao *et al.* doped Cu into ZnO, inducing a synergistic effect that generated abundant oxygen vacancies. These vacancies can not only modulate the local electronic structure of the active sites but also serve as electron-trapping centers, facilitating CO_2 adsorption and promoting electron transfer for its reduction. Additionally, they could also suppress the HER, thereby lowering the energy barrier for electrocatalytic CO_2 conversion to CO, leading to a high FE_{CO} > 80% within a wide potential range.[72] In dual-metal catalysts, the cooperation between the two metals may also lead to the formation of vacancies within certain metal cations. These vacancies, akin to those in anion sites, possess the ability to regulate the electronic structure and also serve as catalytic centers, thereby influencing the adsorption and activation of

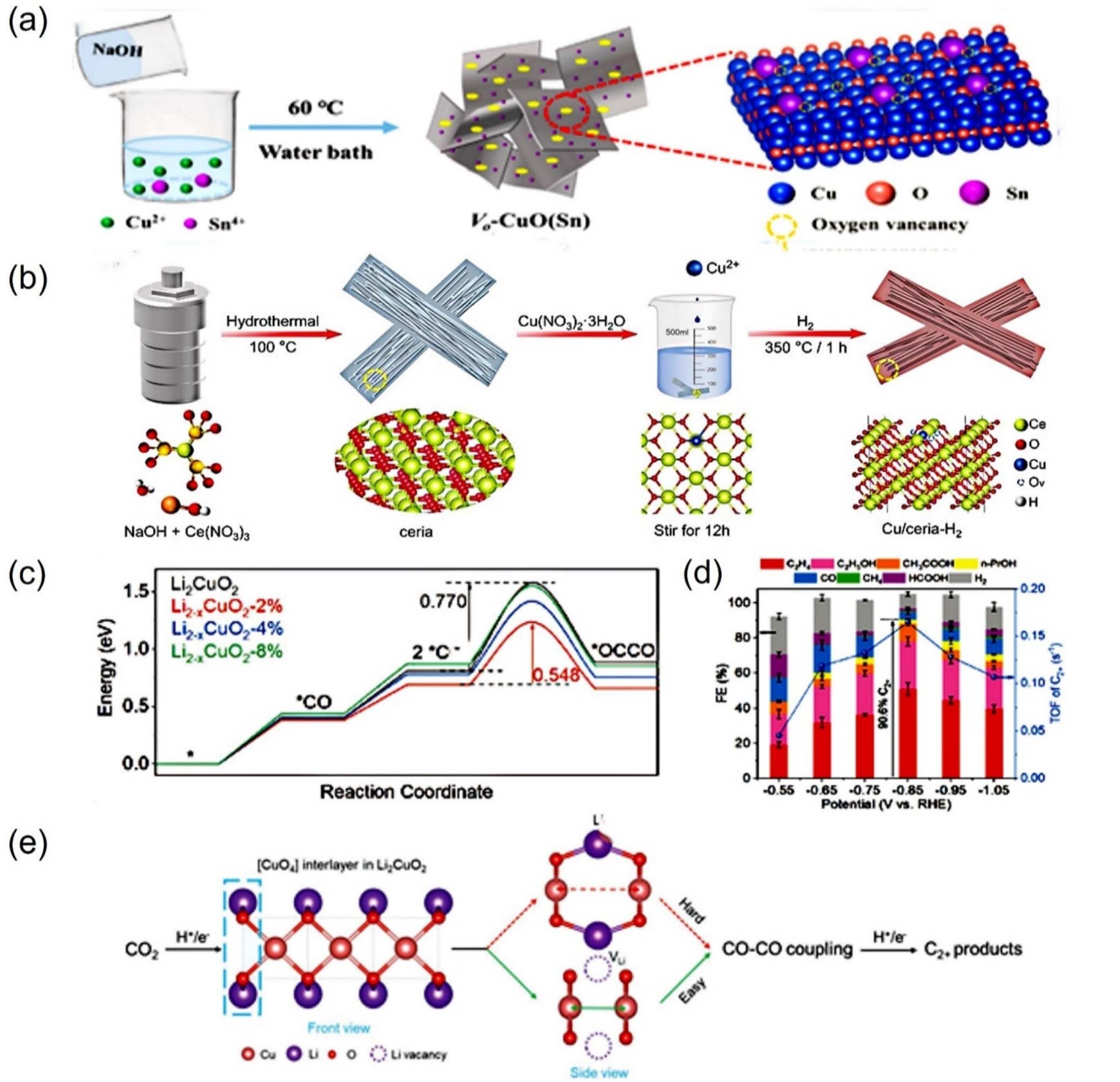

Fig. 2 (a) Schematic illustration of the synthesis of Vo-CuO (Sn). (b) Schematic illustration for the synthesis of the Cu/ceria-H_2 catalyst. (c) Corresponding energy diagrams of C–C coupling for pristine Li_2CuO_2, $Li_{2-x}CuO_2$-2%, $Li_{2-x}CuO_2$-4%, and $Li_{2-x}CuO_2$-8%. (d) Faradaic efficiencies for CO_2RR products and TOF values for C_{2+} products on the $Li_{2-x}CuO_2$ catalyst. (e) Scheme of Li^+ vacancy-tuned [CuO_4] sites that promote C–C coupling. (a) Reproduced with permission.[71] Copyright 2022, American Chemical Society. (b) Reproduced with permission.[70] Copyright 2025, John Wiley and Sons Ltd. (c–e) Reproduced with permission.[73] Copyright 2022, Wiley-VCH Verlag.

CO_2. Zheng, Li, *et al.* incorporated the second metal lithium (Li) into the copper oxides to construct the dual-metal catalyst Li_2CuO_2, constructing Li^+ vacancies, which can tailor the electronic structure and regulate the adsorption energies of intermediate species. It can lower the coordination number of Li^+ around each Cu atom, which highly facilitated the CO–CO coupling, while impeding the competitive HER through suppressing the adsorption of *H intermediates, resulting in the highest FE of 90.6% for C_{2+} products (Fig. 2c–e).[73]

The design and synthesis of dual-metal catalysts containing vacancies with synergistic catalytic effects offer distinct advantages in optimizing the electronic structure of the catalyst and enhancing catalytic efficiency for the CO_2RR. These vacancies not only improve the interaction with reactants but also serve as active sites for catalyzing the CO_2RR. Precise control over the vacancy position, quantity, and type can thus optimize the dual-metal catalyst's electronic structure and performance, offering a novel strategy for efficient CO_2 conversion.

2.1.3 Coordination environment regulation. The regulation of metal coordination environments involves several key aspects, such as the types of central metal sites, the coordination geometry, the coordination number, the type and number of the coordinating atoms, and the first and second coordination shell, each of which can significantly influence the properties and functionalities of dual-metal systems for CO_2 conversion.[74] It is noteworthy that the synergistic interaction between two metals can also modulate the coordination environment of the active metal center, fine-tuning its electronic structure.[33,75] Meanwhile, the regulation of the coordination environment can further enhance the synergistic catalytic effect between metals in dual-metal catalysts, thereby improving the catalyst's ability for the electrocatalytic CO_2RR. Such a modulation not only elucidates the mechanisms of metal interactions but also provides a theoretical basis for designing high-performance catalysts.[76]

Ligands with varying electronegativities such as N, O, S, and P can alter the electron density of metal active centers. For example, electron-withdrawing ligands can lower the energy of metal d-orbitals, weakening intermediate adsorption, while electron-donating ligands can enhance adsorption and promote CO_2 activation.[38,77–79] Voiry *et al.* introduced electron-withdrawing ligand groups such as N_2SN–, N_3N– and C_2N– to tailor the surface coordination environment of a dual-metal Cu–Ag electrocatalyst for CO_2 reduction. Notably, the ligands N_2SN– and N_3N– were found to stabilize the Cu center in a low oxidation state ($0 < \delta < +1$), which critically modulated the electronic structure of the dual-metal Ag–Cu catalyst. This ligand-induced electronic perturbation enhanced the synergistic cooperation between Ag and Cu, promoting CO_2 adsorption and regulating the reduction pathways. Consequently, the optimized catalyst achieved efficient electrocatalytic conversion of CO_2 into high-value multicarbon products (Fig. 3a and b).[80] Zhang *et al.* constructed a redox-active cobalt (Co) protoporphyrin-modified MIL-101(Cr)–NH_2 material for efficient CO_2 electroreduction. The electron-donating ligand –NH_2 group on the coordinated sphere can not only link the Co and Cr sites, increasing the active sites and tuning their electronic structures, but also improve the CO_2 absorption ability, highly optimizing the intermediate *CO binding energy, leading to high CO_2-to-CO conversion (Fig. 3c).[81]

Bridging coordination ligands like N, O, S or halogens can enable electron transfer between the dual metals, creating electron transmission channels, leading to a modified electronic structure and superior catalytic performance for CO_2 reduction.[38] For instance, Zn–N_4-coordinated Cu single atoms in tandem catalysts can facilitate electron flow from Zn to Cu, enhancing CO_2 activation.[82] In another study, Sakamoto, Sekizawa *et al.* developed a robust Br-bridged dinuclear Cu(I) complex, which can efficiently catalyze CO_2 reduction to produce C_3H_7OH with high selectivity. The Br bridge can not only modulate the electronic configurations of the dual Cu active sites by stabilizing their low-spin states, but also strengthen the synergistic collaboration between the bridged Cu centers. This dual modulation mechanism effectively promoted C–C coupling reactions, leading to significantly enhanced C_{2+} hydrocarbon productivity.[83] Chen, Zhang, and colleagues developed a dual-atom catalyst featuring sulfur-bridged Cu–S–Ni motifs. The S-bridge architecture could modulate the electronic charge distribution across the Cu and Ni dual-atom centers, while enhancing synergistic effects between the dual-metal sites. This atomic-level cooperation facilitates the critical COOH* intermediate formation during CO_2 electroreduction, resulting in a remarkable FE of 98.1% for CO production at −0.65 V in a H-cell (Fig. 3d and e).[84]

The synergistic interaction between dual metals, mediated by tailored coordination environments, is critical for optimizing electrocatalytic performance for the CO_2RR. This interaction not only enhances CO_2 adsorption and activation but also promotes favorable reduction pathways, leading to high-value product formation. The regulation of coordination environments has provided a theoretical and experimental basis for designing high-performance dual-metal catalysts, elucidating the mechanisms of metal interactions and improving overall catalytic efficiency. Therefore, the strategic design of coordination environments in dual-metal catalysts, through the careful selection of central metals, ligands, bridging atoms and other coordination parameters, is essential for achieving efficient and selective electrocatalytic CO_2 reduction.

2.2 Geometric structure regulation

Geometric structure regulation is another important aspect of dual-metal catalyst design. By controlling the crystal facet of the metal active sites, the catalyst can be optimized to facilitate the formation of desired products. The incorporation of a second metal can help stabilize these favorable crystal facets, thereby enhancing the catalyst's selectivity for specific products in CO_2 conversion. Additionally, the size of the nanoparticles used in CO_2 reduction can be controlled by the addition of a second metal. Smaller nanoparticles tend to increase the number of active sites and promote the catalytic performance. Morphology regulation is also crucial, as different morphologies such as polyhedra, nanosheets, hierarchical nanoflowers, and porous structures can exhibit unique physicochemical properties that affect the catalyst's performance. By carefully designing the morphology of the dual-metal catalysts through the addition of a second metal, the catalyst can be optimized for high selectivity towards the electrocatalytic CO_2RR.[85,86]

2.2.1 Crystal facet regulation. The crystal facets of cooper materials are regarded as the primary catalytic sites where the electrocatalytic CO_2RR occurs. The type of crystal facets of cooper materials can determine the adsorption energy of CO_2 reduction intermediates, thereby influencing the pathway of the catalytic CO_2 reduction process. Studies have demonstrated a strong correlation between the selectivity of electrocatalytic CO_2RR products and the crystal facets of single-crystal Cu.[87] Specifically, the Cu (100) facet tends to favor the production of C_2H_4, whereas the Cu (111) facet exhibits higher selectivity toward CH_4. In contrast, the Cu (110) facet shows a greater propensity for generating oxygenated hydrocarbons, such as CH_3CH_2OH and CH_3COOH, compared to Cu (100) and Cu

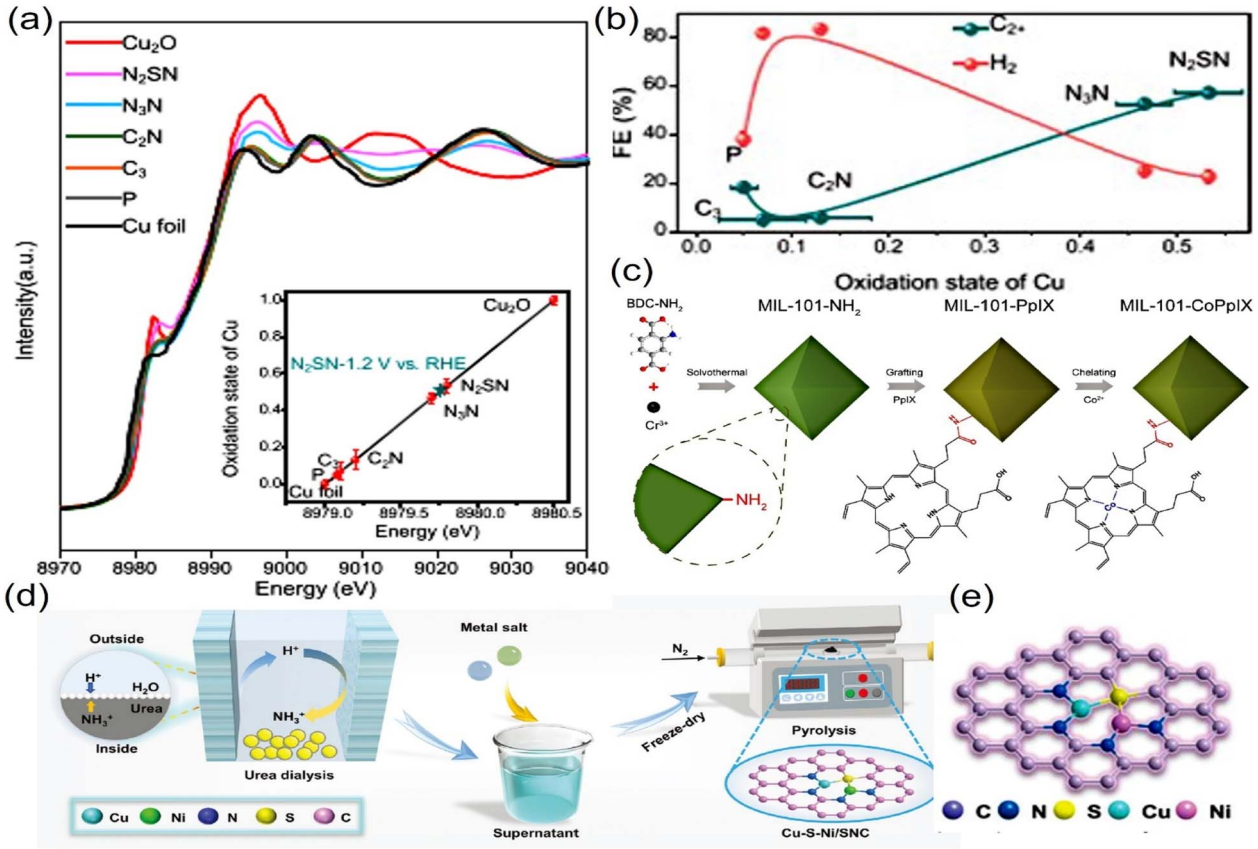

Fig. 3 (a) XANES spectra at the Cu K-edge of the Ag–Cu catalyst. (b) Evolution of the faradaic efficiency for C_{2+} and H_2 measured at −1.2 V *vs.* RHE with the oxidation state of Cu. (c) Synthesis of MIL-101-CoPpIX. (d) Schematic illustration of the synthesis of the Cu–S–Ni/SNC catalyst. (e) Schematic illustration of the synthesis of the Cu–S–Ni/SNC catalyst. (a and b) Reproduced with permission.[80] Copyright 2021, Springer Nature. (c) Reproduced with permission.[81] Copyright, 2024, Elsevier. (d and e) Reproduced with permission.[84] Copyright 2024, Wiley.

(111).[88] However, it is important to note that other byproducts are often generated simultaneously during these processes. To more precisely control the types of crystal facets during the design and synthesis process and further enhance the selectivity of these facets toward desired products, introducing a second metal into copper-based catalysts to form dual-metal catalysts has proven to be a highly effective strategy.[89]

In the design and preparation of dual-metal catalysts, controlling the crystal planes of metal active sites is a crucial step. This strategy focuses on selectively exposing crystal planes that are most favorable for specific chemical reactions, thereby enhancing catalytic performance and significantly promoting the formation of desired products. Specifically, introducing a second metal can stabilize the crystal planes conducive to target product formation, enabling the catalyst to exhibit higher selectivity—preferentially generating the desired product over by-products. The integration of crystal plane regulation with secondary metal incorporation offers an innovative framework for the development of efficient and highly selective catalysts. Fan, Huang, Xi *et al.* achieved well-defined Ag–Cu Janus nanostructures with {100} facets (JNS-100) through the confined growth of Cu on Ag nanocubes (NCs). The introduction of Ag into the Cu catalyst system created a synergistic catalytic effect. DFT calculations revealed that the electronic structure of Ag–Cu JNS-100 was optimized due to the electron transfer from Ag to Cu domains, which enhanced the catalytic activity. The Ag domains efficiently converted CO_2 to CO at lower overpotentials, while the generated CO then spilled over to the adjacent Cu domains, where it was further reduced and C–C coupling was realized toward C_2H_4 production with high efficiency. This tandem mechanism, combined with the exposed {100} facets on the Cu domains, significantly improved the selectivity and efficiency of the CO_2RR toward C_{2+} products. Specifically, the Ag_{65}–Cu_{35} JNS-100 catalyst demonstrated a FE of 54% for C_2H_4 and 72% for C_{2+} products at −1.2 V (*vs.* RHE), outperforming pure Cu nanocubes and physical mixtures of Ag and Cu (Fig. 4a and b).[90] Zheng, Kuang *et al.* successfully incorporated the metal Mg into the Cu catalyst to promote the formation and stabilization of Cu (111) facets, which were particularly effective in promoting C–C coupling, and enhancing the production of ethanol with a high $FE_{ethanol}$ of 76.2 ± 4.8% at 600 mA cm^{-2}. It was found that the Cu (111) facets provided a high density of active sites and optimal adsorption energies for key intermediates such as *CO. These facets also lowered the energy required for *CO–CO coupling, and improved the stabilization of the *CHCHOH intermediate, which were critical for ethanol production. Moreover, the synergistic effect between Cu and Mg in the dual-metal material

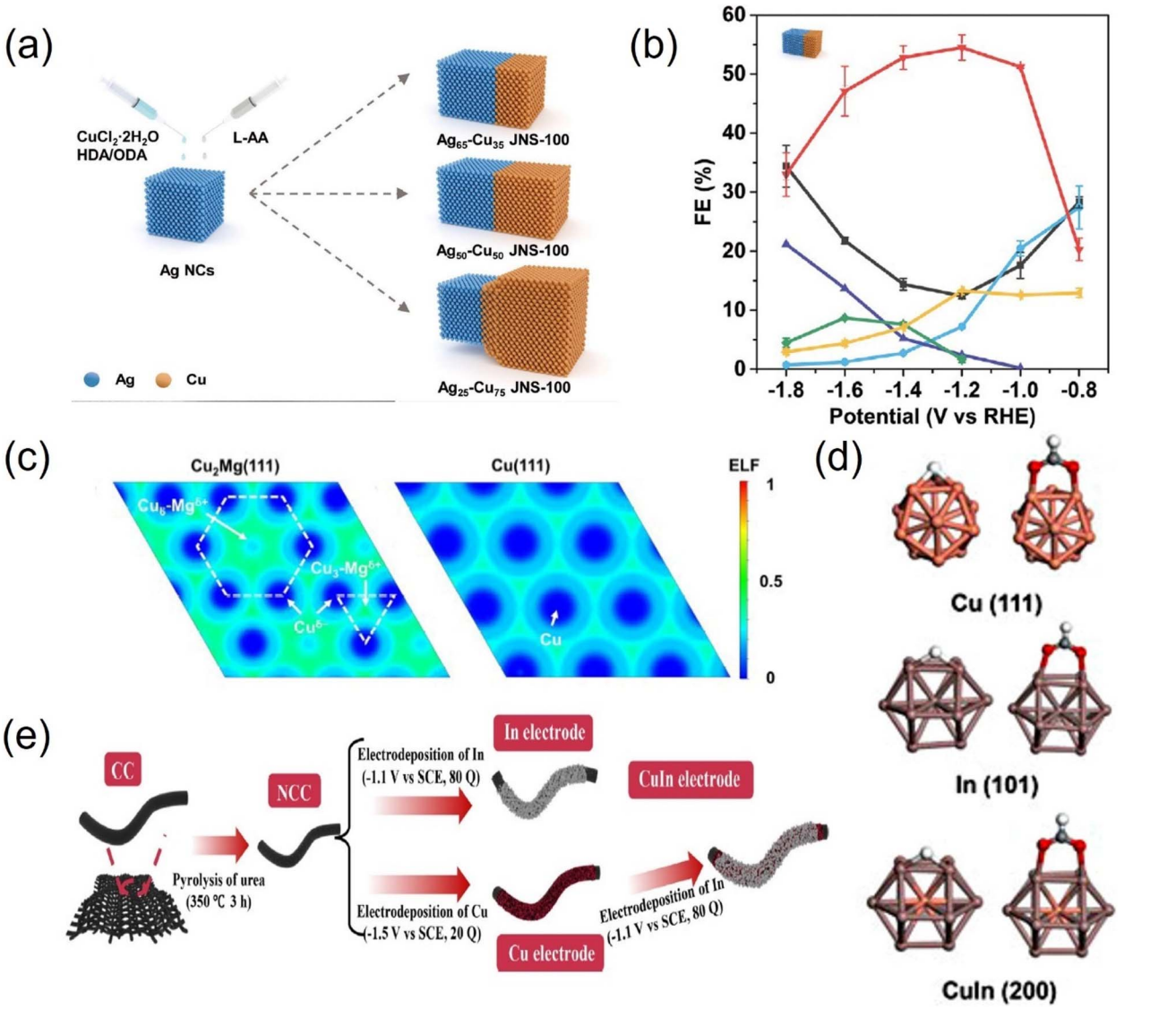

Fig. 4 (a) Schematic illustration for the synthesis of three kinds of Ag–Cu JNS-100. (b) Faradaic efficiencies (FEs) for CO_2RR products obtained on Ag_{65}–Cu_{35} JNS-100. (c) Electronic localization function of Cu_2Mg (111). (d) Optimized structure of cluster Cu (111), cluster In (101), and cluster CuIn alloy (200). (e) Schematic diagram of the fabrication process of the CuIn electrode. (a and b) Reproduced with permission.[90] Copyright 2021, Wiley. (c) Reproduced with permission.[91] Copyright 2023, John Wiley and Sons Ltd. (d and e) Reproduced with permission.[92] Copyright 2023, Elsevier.

facilitated the electron transfer from Mg to Cu, leading to a negative shift in the d-band center compared to that of commercial Cu, indicating a more favorable electronic environment for C–C coupling (Fig. 4c).[91]

In addition to the conventional approach of modulating copper crystal facets, such as the (100) plane, the regulation of other types of metal facets through the synergistic effect of dual-metal systems is also considered as a promising approach for enhancing the electrocatalytic CO_2RR. Qiao, Zhang and their team developed CuIn dual-metal catalysts featuring co-exposed CuIn (200) and In (101) facets, which exhibited a high FE up to 80% for formate production at relatively low overpotentials, along with high stability. They discovered that the synergistic effect of the two metals played a crucial role, where the CuIn (200) facet can specifically reduce the overpotential for formate production, while the In (101) facet can enhance the overall CO_2 adsorption capacity. Density functional theory (DFT) calculations further revealed that the CuIn (200) and In (101) lattice facets collaborate to stabilize the key OCHO* intermediate (Fig. 4d and e).[92] Xiong *et al.* achieved highly efficient electrocatalytic CO_2RR to produce formate by fabricating dual-metal Bi_5In_5 nanofibers (NFs) with precise control over the growth of InBi (200) crystal facets, through a synthetic approach combining electrospinning and electrochemical reduction techniques. It was found that attributed to the dual-metal sites formed by In and Bi atom, the (200) crystalline plane of Bi_5In_5 could promote the electrocatalytic CO_2RR process by strongly adsorbing the key *OCHO intermediate and reducing the

reaction energy barrier, thereby enhancing catalytic selectivity for HCOOH production.[93]

In summary, the precise regulation of crystal facets in dual-metal catalysts has emerged as a highly effective approach to enhance the selectivity and efficiency of electrocatalytic CO_2 reduction. By tailoring specific facets and leveraging synergistic effects in dual-metal systems, remarkable control over reaction pathways has been achieved, enabling high FE for target products. These advancements highlight the critical role of facet engineering in optimizing intermediate adsorption and lowering energy barriers for key steps.

2.2.2 Size regulation. The size of dual-metal catalysts such as dual-atoms, clusters and nanoparticles governs their electrocatalytic CO_2RR performance by balancing atomic efficiency, intermediate binding, and reaction pathways.

As for dual-atom catalysts (DACs) consisting of two heterometallic active centers, they represent an emerging class of electrocatalysts that combine the advantages of single-atom catalysts (SACs) and subnanometer clusters for the CO_2RR. By precisely engineering dual-metal sites, DACs can achieve maximized metal atom utilization while enabling synergistic electronic and geometric effects that are unattainable with isolated SACs or larger clusters.[94] Lu, Liu, *et al.* employed a molten-salt-assisted strategy to synthesize Fe–Zn dual-atom catalysts (FeZnNC) on N-doped carbon supports. The study demonstrated that due to the electronegativity difference between Fe and Zn (Fe: 1.83; Zn: 1.65), electrons preferentially transferred from Zn to Fe, which resulted in charge redistribution and modified electronic environments of the two active sites, creating optimal conditions for the CO_2-to-CO conversion pathway. The synergistic effect of dual-atom catalysts entailed the Zn site functioning as the primary active center for CO_2 activation and *COOH intermediate formation, with the Fe site stabilizing intermediates and weakening *CO binding to avert site poisoning, thereby achieving $FE_{CO} > 94\%$ in acidic media at industrial current densities ranging from 100 to 400 mA cm^{-2} (Fig. 5a and b).[95] Wang *et al.* developed a heterodimetallic Co–Ni–N–C dual-atom catalyst with neighboring Co–Ni diatomic sites, which attained a remarkable CO yield rate of 53.36 mA mg $cat.^{-1}$, along with an outstanding FE_{CO} of 94.1%. DFT calculations have revealed that the Co–Ni synergistic catalysis mechanism for the CO_2RR entails the effective activation of CO_2 at dual Co–Ni sites and also the formation of CO *via* optimized pathways where another CO_2 molecule undergoes reduction while a CO* intermediate remains adsorbed at the site (Fig. 5c and d).[96]

The metal clusters bridge atomic and nanoscale catalysts, as their well-defined yet tunable structures – ranging from a few to dozens of metal centers – combine atomic-level precision with nanoparticle-like ensemble effects. They can offer superior metal utilization like atomic catalysts, while avoiding the low metal loading limitations of atomic catalysts. Moreover, their multinuclear active sites can mimic the selectivity of nanoparticles, enabling tailored control over the C–C coupling reaction pathway for the CO_2RR. The dual-metal clusters can offer superior catalytic performance compared to their monometallic systems by synergistically integrating the properties of different metal components, which can modify charge distribution and orbital hybridization, enabling precise optimization of intermediate binding energies for enhanced electrocatalytic CO_2RR activity.[97] Zhu, Jin, Du, *et al.* precisely engineered the structures of dual-metal clusters (Au_8Ag_{55}, Au_8Ag_{57}, and $Au_{12}Ag_{60}$) with different sizes, which enabled tailored catalytic performance for the CO_2RR by manipulating geometric properties at the atomic level. They discovered that the smaller Au_8Ag_{55} NC exhibits a distinctive charge segregation phenomenon, where electrons preferentially gather around the core Au atoms while inducing an electron-deficient condition on the outer Ag atoms. This reduction in electron density on the Ag atoms effectively diminishes the competition from the HER, thereby enhancing the CO_2RR process (Fig. 5f).[98] Metal–organic frameworks (MOFs) are unique cluster-based materials, in which atomically precise metal clusters are interconnected by well-ordered organic ligands, enabling outstanding electrocatalytic CO_2RR performance. Lu, Francisco, Han, Zhu, *et al.* successfully constructed a Cu–Ni dual-metal MOF cluster with an asymmetric structure modulated by a pyrazolate ligand, namely Cu_1Ni–BDP, which achieved a high CO_2-to-C_2H_4 conversion with a FE of 52.7% along with great stability. DFT calculations revealed that electron transfer from Cu to Ni generates electron-deficient Cu and electron-rich Ni sites in the asymmetric Cu_1Ni cluster. The unique asymmetric Cu–Ni electronic configuration creates synergistic effects that precisely modulate *CO adsorption energy while reducing the activation barrier for *COH–COH formation, thereby enabling exceptional CO_2 reduction performance (Fig. 5e).[99]

In addition to dual-metal atomic catalysts and dual-metal clusters, the size regulation of dual-metal nanoparticle catalysts also has a significant impact on electrocatalytic CO_2 reduction. Although bulkier nanoparticles suffer from decreased atomic utilization efficiency, the complex surface architecture containing multiple active site types can directly offer high catalytic performance towards the CO_2RR. Chen, Feng, *et al.* innovatively designed dual-metal ZnO/Ag twinned-phase ultrasmall nanoparticles (≤3 nm) uniformly embedded in a nanoporous carbon matrix, achieving 60.9% energy conversion efficiency for CO production with exceptional stability over six days. They discovered that nanopore confinement ensures the small particle size of the catalysts, leading to high active site density and agglomeration resistance. DFT calculations revealed that the charge redistribution from Zn/Ag to O atoms preferentially stabilizes the *COOH intermediate while energetically disfavoring competing HCOO* and *H pathways, resulting in highly selective (98.1%) CO production.[100] Byon, Yang, *et al.* developed a series of dual-metal Cu_xIr_{1-x} alloy nanoparticles with a small size of about 1.6 nm, which could achieve unprecedented performance in CO_2-to-*t*-BuOH conversion, delivering a FE of 14.8%—very high C_4 production. Studies revealed that the high C_4 selectivity arises from the synergistic Cu–Ir interaction, combined with the oxophilic nature of the Ir-rich surface, which stabilizes critical oxygen-bound intermediates (*e.g.*, CH_2CHO*, CH_3CHO, and CH_3CH_2O) and thereby boosts CO_2 reduction efficiency.[63]

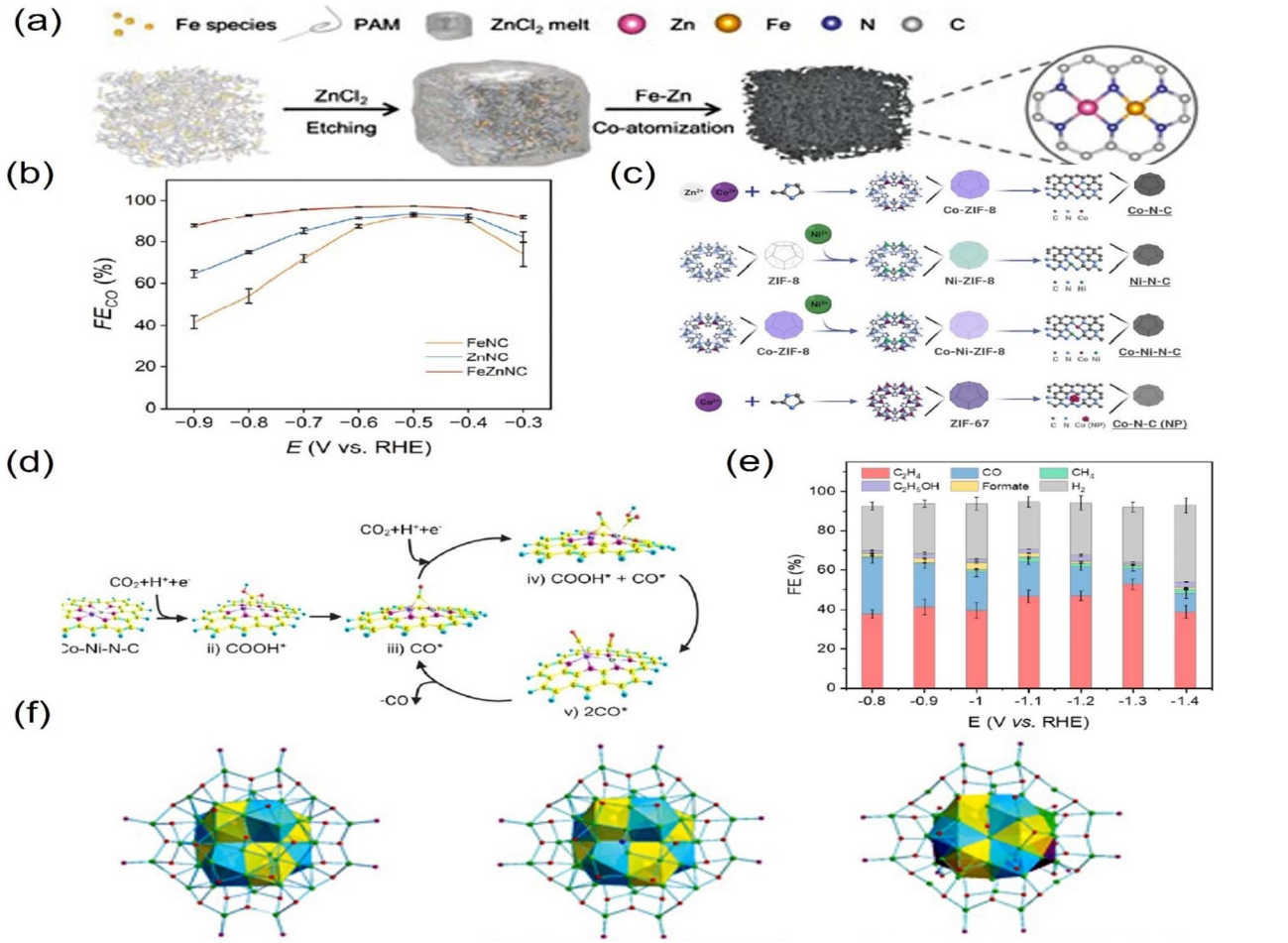

Fig. 5 (a) Scheme diagram for the synthesis of a dual-atom FeZnNC catalyst. (b) Faradaic efficiencies of CO at different potentials by using FeZnNC. (c) Schematic diagram of the fabrication process of Co–N–C, Ni–N–C, Co–Ni–N–C, and Co–N–C (NP) (NP: nanoparticle). (d) Catalytic pathway on the dual Co–Ni site based on the optimized structures of adsorbed intermediates COOH*and CO*. (e) Faradaic efficiencies for CO_2RR products and H_2 on the Cu_1Ni–BDP MOF at different cathode potentials. (f) Total structure of Au_8Ag_{55}, Au_8Ag_{57}, and $Au_{12}Ag_{60}$ NC. (a and b) Reproduced with permission.[95] Copyright 2024, John Wiley and Sons Inc. (c and d) Reproduced with permission.[96] Copyright 2024, the Royal Society of Chemistry. (e) Reproduced with permission.[99] Copyright 2023, Wiley-VCH Verlag, Wiley. (f) Reproduced with permission.[98] Copyright 2023, American Chemical Society.

The size regulation of dual-metal catalysts is a powerful lever to tailor the synergistic effect on catalytic properties for the electrocatalytic CO_2RR. The interplay of electronic and geometric effects across scales will drive advancements in high-performance CO_2RR catalysts.

2.2.3 Morphology regulation. Morphological regulation is pivotal for designing efficient dual-metal catalysts for the electrocatalytic CO_2RR. Precisely engineering morphological architectures, such as shape control and porous regulation could optimize surface area, active site accessibility, electronic interactions, and mass transport efficiencies, thereby offering unprecedented catalytic performance with superior activity, selectivity, and operational stability. The integration of morphological engineering and dual-metal composition optimization emerges as a pioneering strategy for designing catalysts that enable industrial-scale CO_2 conversion.[101]

By utilizing the modulation of two unique metals, dual-metal catalysts can be morphologically optimized into diverse nanostructures, ranging from distinct shapes like polyhedra, nanosheets, hierarchical nanoflowers or dendrites, to porous structures like core–shell or hollow structures. This approach enhances mass transport efficiency and promotes electrolyte infiltration during the CO_2RR by establishing directional charge/mass transfer pathways and increasing the surface area available for reactant interaction.[102,103]

Polyhedral structures in nanomaterials offer numerous advantages that make them highly attractive for various applications. The unique shape and arrangement of atoms in polyhedral nanomaterials often lead to tailored electronic properties and enhanced catalytic activity for the electrocatalytic CO_2RR.[104] For instance, Zhang, Wang, and colleagues reported that the incorporation of Ag into Cu_3N nanocubes (NCs) leads to a well-defined nanocube (NC) structure, where Ag atoms are successfully integrated into some Cu sites within the Cu_3N unit cell, resulting in Cu_3N–Ag NCs. The dual Ag–Cu sites exhibit a cascade catalysis strategy that markedly boosts the

electrochemical CO_2 reduction process, resulting in significantly enhanced FE and partial current density for C_2H_4 production, which are much higher compared to those of pure Cu_3N nanocubes (NCs). They discovered the synergistic effect between Cu and Ag, wherein the relatively weak binding strength of *CO on Ag sites aids in the generation and subsequent transfer of CO species to Cu sites. At these Cu sites, the elevated local CO coverage promotes asymmetric C–C coupling, leading to the formation of key intermediate species *COCHO (Fig. 6a).[48] In another example, Gong's group reported that incorporating dual-metal doping into catalytic materials presents a potent strategy for modulating their structural attributes and substantially impacting the efficiency of electrocatalytic CO_2 reduction. By adjusting the ratios of Cu and Pd precursors, diverse morphological transformations of Pd–Cu nanocrystals (NCs) can be realized, spanning from concave rhombic dodecahedra to flower-like structures. The flower-like Pd_3Cu (FL-Pd_3Cu), composed of {111} and high-index step facets, contributed to their high selectivity for CO production. Conversely, the concave rhombic dodecahedral Cu_3Pd (CRD-Cu_3Pd) exposed high-index facets, which have demonstrated a reduced onset potential and increased current density for CH_4 production compared to Cu foil. They discovered that attributed to the synergistic effects of Cu and Pd as well as the exposure of high-index facets, CRD-Cu_3Pd offered more low coordinated active sites and modified the binding energies of reaction intermediates such as *CHO, thereby enhancing its catalytic performance for CH_4 production (Fig. 6b).[105]

Due to their two-dimensional (2D) confinement and ultrathin nature, nanosheets exhibit an enormously high surface area-to-volume ratio, which often leads to unique properties such as high carrier mobility and tunable band gaps, which are particularly advantageous for the electrocatalytic CO_2RR.[106,107] Wang and Che's group reported that metals like Co, In and Ru were successfully introduced into Bi materials *via* a facile hydrolysis method, resulting in the formation of metal-doped Bi nanosheets with unique structural and chemical properties compared to pristine Bi nanosheets. Notably, the $Co_{0.05}$–BOON nanosheets significantly enhanced the electrocatalytic reduction of CO_2 to HCOOH, thanks to the synergistic effect between cobalt and bismuth. The incorporation of cobalt atoms into the bismuth nanosheets modulated the electronic structure *via* electron transfer, leading to a high selectivity (~90%) and stability for HCOOH production over 100 hours at 100 mA cm^{-2}. Moreover, the Co-doped Bi (012) surface exhibited stronger binding energy towards the key OCHO* intermediates, facilitating the efficient conversion of CO_2 to formic acid at a lower applied potential compared to the pure Bi surface (Fig. 6d).[108] In another study, Zhang and colleagues reported on the $CuMnO_2$ nanosheet structure, wherein the controlled synthesis method introduced Cu and Mn, yielding a material abundant in oxygen vacancy defects. The abundant oxygen vacancies in the $CuMnO_2$-Vo nanosheets effectively shift the d-band center of the active Mn sites upwards. The synergistic effect of Cu and Mn in the $CuMnO_2$ nanosheets, coupled with the presence of oxygen vacancies, significantly enhances the adsorption strength of the active sites for the intermediates *COOH and *CO, resulting in a high FE for ethylene production (93.4% at −1.0 V *vs.* RHE) and excellent stability over 192 hours (Fig. 6c and e).[109]

The branching structure of dendrites and the layered petals of nanoflowers offer excellent mass transport pathways, which can facilitate the efficient diffusion of CO_2 to the active sites and the removal of reduction products from the catalyst surface, reducing mass transfer limitations and enhancing the overall reaction rate for the CO_2RR.[110–112] Liu *et al.* reported that the integration of Cu and Sn into the Cu_1SnS_2 catalyst leads to the formation of a unique microflower-like nanostructure, creating a hierarchical architecture with multiple layers and pores. The doping of Cu into SnS_2 not only modifies the electronic structure of the material but also plays a pivotal role in shaping its morphological features. The *operando* detections confirmed that the incorporation of a single Cu atom into the Cu_1/SnS_2 catalyst could promote the reduction of SnS, resulting in the formation of Cu_1/Sn during the CO_2RR. This dynamic transformation effectively boosts the generation of CO_2^-/OCHO intermediates. DFT calculation found that Cu_1 and Sn work together as active sites to reduce the Gibbs free energy for the formation of the *OCHO intermediate, facilitating the conversion of CO_2 to formate (Fig. 6f).[113] In another example, Lu, Jiao, *et al.* constructed a $Bi_2O_{3-x}/Mg(OH)_2$ catalyst with a nanoflower-like structure, which can increase the surface area of the catalyst, providing more active sites for CO_2 adsorption and reduction even for low-concentration CO_2. They discovered that the dual-active-site catalyst leverages a synergistic effect between the bismuth oxide active sites and the magnesium hydroxide basic sites, in which a Lewis-base active site can facilitate the enrichment and activation of CO_2, along with a highly selective catalytic site dedicated to CO_2 conversion, leading to a high formic acid selectivity exceeding 97% across a wide potential range (Fig. 6g).[114] There are also many dual-metal catalysts with dendrite structures for the electrocatalytic CO_2RR, which exhibit excellent catalytic performance. For instance, Schultz *et al.* reported a dual-metal catalyst Ag/Cu_2O with dendritic morphology, in which the combination of Ag and Cu_2O leads to selective photoelectrochemical CO_2 reduction to acetate, with a high FE of 54%. It was found that the Ag/Cu_2O nanodendrite structure exhibits a unique combination of plasmonic and semiconductor properties that synergistically enhance the CO_2 reduction reaction. The *in situ* tests revealed that the reaction rate entails the transfer of a single electron from the electrode to CO_2, leading to its reduction into the $*CO_2^-$ radical anion and subsequently generating adsorbed CO, which acts as a vital intermediate in the process of C–C coupling for acetate production (Fig. 6i).[115]

The porous structures like core–shell or hollow structures can not only offer a larger surface area and more active sites compared to their bulk counterparts, but also enhance CO_2/product diffusion, significantly reducing mass transfer limitations.[116,117] For instance, Zeng, Tuo, *et al.* developed a group of dual-metal Ag@Cu_2O core–shell nanoreactors featuring adjustable Cu_2O shell thicknesses, displaying a volcano-like pattern in the generation of C_{2+} products, in which Ag@Cu_2O-40 with medium thickness exhibited the highest FEC_{2+} of

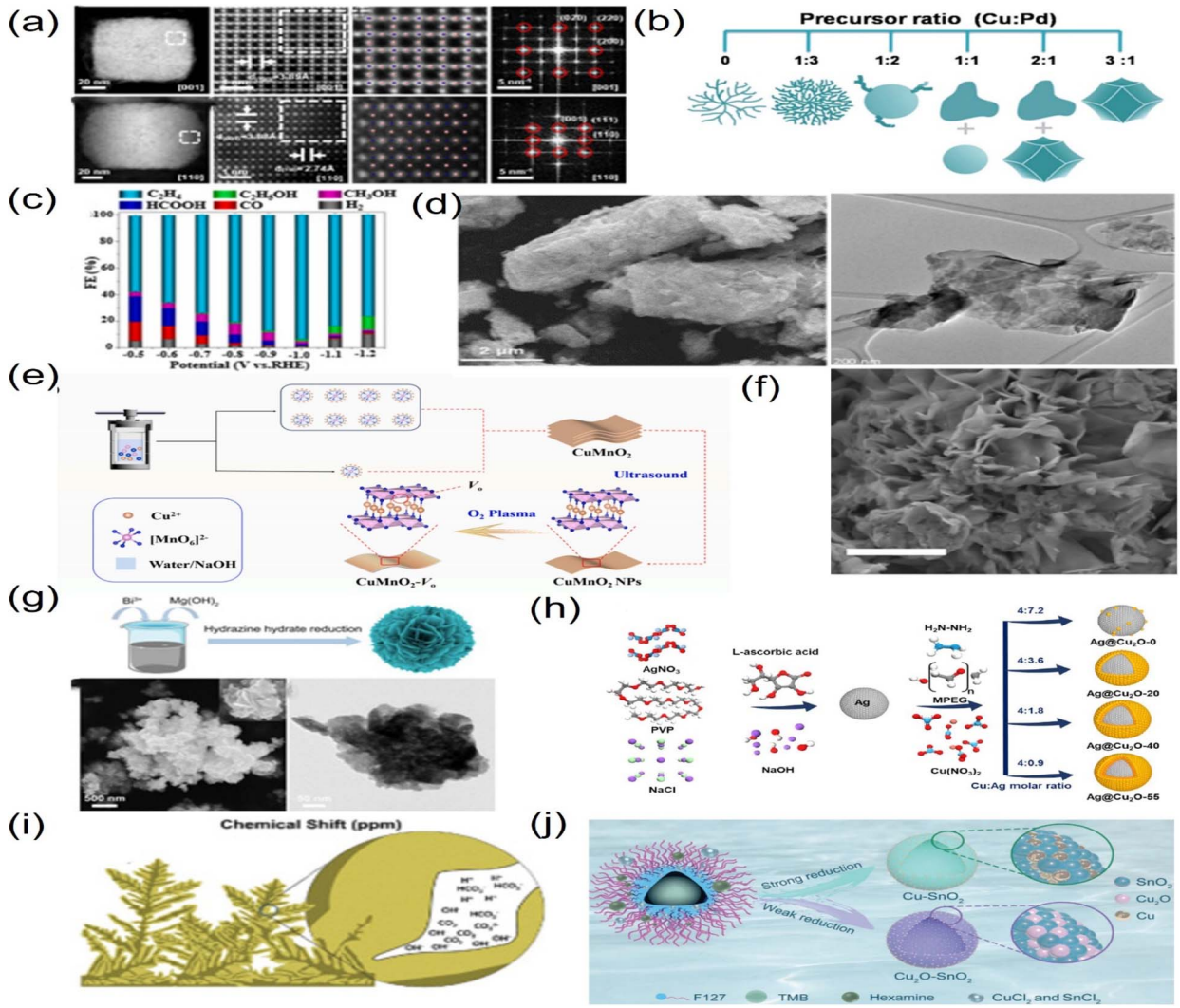

Fig. 6 (a) Structural characterization of Cu_3N–Ag NCs. (b) Morphological evolution of Pd–Cu catalysts with different compositions. (c) Faradaic efficiencies for CO_2RR products by using $CuMnO_2$. (d) Structural characterization of $Co_{0.05}$–BOON. (e) Synthesis schematic of $CuMnO_2$-Vo. (f) SEM image of Cu_1/SnS_2. (g) Synthesis and characterization of dual-active site catalyst $Bi_2O_{3-x}/Mg(OH)_2$. (h) Schematic illustration for the synthesis of Ag@Cu_2O cascade nanoreactors. (i) Representative scheme of the microenvironment of Ag/Cu_2O during the CO_2 reduction process. (j) Schematic illustration for synthesizing Cu–Sn-based catalysts in the CO_2RR. (a) Reproduced with permission.[48] Copyright 2024, American Chemical Society. (b) Reproduced with permission.[105] Copyright 2017, Wiley-VCH Verlag. (c and e) Reproduced with permission.[109] Copyright,2025, Elsevier. (d) Reproduced with permission.[108] Copyright 2024, John Wiley and Sons Ltd. (f) Reproduced with permission.[113] Copyright 2024, American Chemical Society. (g) Reproduced with permission.[114] Copyright 2025, Springer. (h) Reproduced with permission.[103] Copyright 2023, American Chemical Society. (i) Reproduced with permission.[115] Copyright 2024, American Chemical Society. (j) Reproduced with permission.[118] Copyright 2024, Wiley.

78.5%. The combination of Ag and Cu_2O in a core–shell structure leads to synergistic effects, in which the CO generated at the Ag core spills over to the Cu_2O shell, where it promotes the C–C coupling for C_{2+} production. They discovered that the porous Cu_2O shell creates a confined space around the Ag core, promoting the local accumulation of CO intermediates. Meanwhile, the short diffusion pathways between the Ag core and Cu_2O shell minimize the loss of reactive intermediates, ensuring efficient utilization of CO for subsequent C–C coupling (Fig. 6h).[101] As for the hollow structure, Sun, Zhang, *et al.* developed two dual-metal Cu–Sn oxide based catalysts Cu–SnO_2 and Cu_2O–SnO_2 with hollow spherical structures, of which the former was obtained under strong reduction conditions, while the latter was obtained under weaker reduction conditions. The findings reveal that the Cu–SnO_2 catalyst exhibits remarkable selectivity towards ethanol, achieving a selectivity of 74.6%, while the Cu_2O–SnO_2 catalyst shows high selectivity towards ethylene, with a value of 71.4%. This underscores the crucial role played by the distinct interphases formed between Cu/Cu_2O and SnO_2 in determining the product distribution, demonstrating a significant impact on the catalytic outcomes. DFT calculations uncovered that the Cu–SnO_2 interphase features robust electron interactions, facilitating the generation of essential intermediates such as *COH, which favors

Table 1 Summary of state-of-the-art dual-metal catalysts for the electrocatalytic CO_2RR into C_1 products

Catalyst	Dual metals	FE of C_1 products (%)	Current density j_{C1} (mA cm^{-2})	Electrolyte	Ref.
Vo-CuO(Sn)	Cu and Sn	99 (CO)	38.65	0.1 M $KHCO_3$	71
Cu/CeO_2	Cu and Ce	70.03 (CH_4)	150	1 M KOH	63
Cu–ZnO	Cu and Zn	80 (CO)	45	0.1 M $KHCO_3$	65
MIL-101-CoPpIX	Co and Cr	97.1 (CO)	5	0.1 M $KHCO_3$	81
Cu–S–Ni/SNC	Cu and Ni	98.1 (CO)	550	0.5 M $KHCO_3$	84
CuIn	Cu and In	80 (HCOOH)	13.84	0.5 M $KHCO_3$	92
Bi_5In_5	Bi and In	96.8 (HCOOH)	250.9	0.1 M $KHCO_3$	93
FeZnNC	Fe and Zn	94 (CO)	100	1 M KOH	95
Co–Ni–N–C	Co and Ni	94.1 (CO)	13.34	0.1 M $KHCO_3$	88
Au_8Ag_{55}	Au and Ag	66 (CO)	23	0.5 M $KHCO_3$	98
ZnO–Ag@UC	Zn and Ag	98.1 (CO)	22.3	0.5 M $KHCO_3$	100
Pd–Cu	Cu and Pd	40.6 (CH_4)	16.7	0.1 M $KHCO_3$	105
$Co_{0.05}$-BOOM	Co and Bi	~90 (HCOOH)	200	1 M KOH	108
Cu_1/SnS_2	Cu and Sn	~90.9 (HCOOH)	158	0.5 M $KHCO_3$	113
Bi_2O_{3-x}/Mg(OH)2	Bi and Mg	97 (HCOOH)	140	0.5 M $KHCO_3$	114
Ni_2-NCNT	Ni andNi	97 (CO)	76	0.5 M $KHCO_3$	126
Ni_2/N-CNTs	Ni and Ni	90.7 (CO)	64.5	0.5 M $KHCO_3$	118
Fe_2–N–C	Fe and Fe	80 (CO)	32.04	0.5 M $KHCO_3$	128
Ni–Cu	Cu and Ni	~99 (CO)	235	Phosphate buffer, 1 M KOH and 0.5 M $KHCO_3$	122
Co–Cu DASC	Cu and Co	99.1 (CO)	483	0.5 M $KHCO_3$	132

Table 2 Summary of state-of-the-art dual-metal catalysts for the electrocatalytic CO_2RR into C_{2+} products

Catalyst	Dual metals	FE of C_{2+} products (%)	Current density j_{C2+} (mA cm^{-2})	Electrolyte	Ref.
Cu_xIr_{1-x}	Cu and Ir	14.8 (*t*-BuOH)	0.207	0.1 M $KHCO_3$	63
$Cu/CaCO_3$	Cu and Ca	83.7	393	1 M KOH	64
Li_2CuO_2	Cu and Li	90.6	706	1 M KOH	73
Ag–Cu	Cu and Ag	80	261.1	0.5 M $KHCO_3$	81
Ag_{65}–Cu_{35} JNS-100	Cu and Ag	72	15.14	0.1 M $KHCO_3$	90
$Cu_2Mg(111)$	Cu and Mg	76.2	720	1 M KOH	91
Cu_1Ni–BDP	Cu and Ni	52.7	500	1 M KOH	99
Cu_3N–Ag	Cu and Ag	36.6	26.7	1 M KOH	48
$CuMnO_2$	Cu and Mn	93.4	14.57	0.1 M $KHCO_3$	109
$Ag@Cu_2O$-40	Cu and Ag	78.5	20	1 M KOH	103
Cu/Cu_2O–SnO_2	Cu and Sn	74.6	8.7	0.1 M $KHCO_3$	118
Cu2	Cu and Cu	51	496.4	1 M KOH	122
BiCu-SAA	Cu and Bi	73.4	400	1 M KOH	140
Cu_xGa_x	Cu and Ga	83	1000	1 M KOH and 0.5 M $KHCO_3$	141
CoCu composite	Cu and Co	71.1	26.7	0.1 M $KHCO_3$	52
CuO + Ni-surface	Cu and Ni	55.2	199	0.1 M $KHCO_3$	62
B–Cu–Zn	Cu and Zn	79	200	1 M KOH	60
Ag/Cu_2O–Cu	Cu and Ag	76.5	1000	1 M KOH	145
Cu/Ag	Cu and Ag	~80	356.7	1 MKOH	136
Au–Cu Janus NSs	Cu and Au	67	290	3 M KOH	149

asymmetric C–C coupling to yield ethanol. Conversely, the Cu_2O–SnO_2 interphase is characterized by the presence of oxygen vacancies at both sites, enhancing the abundance of *CO intermediates, thereby promoting symmetric C–C coupling to produce ethylene (Fig. 6j).[118]

Precise morphological control in dual-metal catalysts—ranging from polyhedra and nanosheets to hierarchical and porous architectures—enables tailored electronic and geometric effects that govern intermediate binding, C–C coupling, and mass transport. This structural diversification, coupled with synergistic metal interactions, paves the way for industrial-scale CO_2 conversion with target-product selectivity.

3 Influence of different types of dual-metal active sites with synergistic effects on the mechanism

The incorporation of dual-metal active sites in catalysts represents a highly effective strategy for enhancing catalytic performance, particularly in the field of electrocatalytic CO_2 reduction (Tables 1 and 2). The synergistic interactions between dual-metal sites can optimize reaction pathways, significantly improving catalytic activity, selectivity, and stability. Based on the size scale and structural characteristics of the active sites,

dual-metal active sites can be categorized into dual-atom metal catalysts and dual-metal nanoparticle catalysts.[119]

Dual-atom metal catalysts are composed of two isolated metal atoms, typically anchored on supports such as nitrogen-doped carbon or metal–organic frameworks. Their catalytic performance is finely tuned through electronic coupling and spatial proximity. The catalytic mechanism relies on atomic-level precision and the synergistic effects of dual-metal sites, particularly electronic synergy, which optimizes the adsorption of intermediates by modulating the d-band center. Specifically, electron transfer between the two metal atoms shifts their respective d-band centers, fine-tuning the adsorption strength: for instance, an upward shift in the d-band center of one metal atom enhances adsorption, while the other balances the adsorption strength through electron transfer or orbital hybridization, preventing efficiency loss caused by excessively strong or weak adsorption. In contrast, dual-metal nanoparticle catalysts feature active sites at the nanoscale (1–100 nm), with their catalytic performance governed by a combination of electronic effects, geometric effects, and interface effects. These include the optimization of intermediate adsorption through surface modification and electron transfer. Dual-atom metal catalysts demonstrate high selectivity in reduction reactions, predominantly yielding single products such as CO, while dual-metal nanoparticle catalysts are better suited for complex reactions, enabling the reduction of CO_2 to a variety of hydrocarbons.[120]

3.1 Dual-atom metal synergistic catalysis for the electrocatalytic CO_2RR

Dual-atom catalysts (DACs), characterized by their exceptional atomic efficiency, precisely defined electronic structures, and unique dual-atom synergistic effects, have risen as prominent candidates for electrocatalytic CO_2 reduction. The precise arrangement of two metal atoms in DACs can create specific catalytically active sites with synergistic effects, which can lower the activation energy of the reaction, thereby accelerating the rate of CO_2 reduction. DACs can be further distinguished into homonuclear and heteronuclear types, each offering unique advantages for their applications for the electrocatalytic CO_2RR. Hence, in this section, we will explore the impact of synergistic catalysis between dual metal atoms on the efficiency and catalytic mechanism of electrocatalytic CO_2 reduction, highlighting the distinct roles of homonuclear and heteronuclear dual-metal configurations.[43]

3.1.1 Homo-dual atom synergistic catalysis. Homonuclear dual-atom catalysts (DACs) have emerged as a groundbreaking class of materials in electrocatalytic CO_2 reduction, demonstrating superior catalytic performance compared to their single-atom counterparts. This enhanced performance is primarily attributed to the cooperative effects between dual metal active sites, which enable precise control over reaction pathways and intermediate stabilization.[121] The present study focuses on structural optimization through strategic regulation of metal types like Ni_2, Fe_2, Cu_2 and their coordination environments, aiming to achieve efficient conversion of CO_2 into CO or hydrocarbons.[122,123] The synergistic mechanism of homonuclear DACs operates through a dual modulation of electronic and geometric effects, playing a pivotal role in determining the adsorption strength of key intermediates of CO_2 reduction.

Nickel, with its moderate d-band center position and rich valence state variability, is an ideal candidate for constructing highly efficient CO_2 reduction catalysts. Particularly in homonuclear dual-atom configurations, the synergistic interaction between two nickel atoms creates a uniform and consistent electronic effect, significantly enhancing catalytic performance. In this research direction, Lu's group has made systematic contributions. Among the pioneering studies in this field, Lu and colleagues achieved a significant breakthrough for the electrocatalytic CO_2RR in 2018 with the development of a dinuclear nickel complex, Ni_2L_1 (L_1 = 1,2-bis((5,7-dimethyl-1,4,8,11-tetra-azacyclotetradecan-6-yl)methyl)benzene). This catalyst demonstrated remarkable performance in CO_2 reduction, achieving a FE_{CO} of 95%, a turnover number (TON) of 4.1×10^6, and an impressive turnover frequency (TOF) of 190.0 s^{-1}. The outstanding performance of complex Ni_2L_1 compared to mononuclear Ni molecular catalysts for the CO_2-to-CO conversion stems from the synergistic catalytic effect between its two Ni centers. It was found that one Ni center can serve as a Lewis base, donating an electron to the CO_2 molecule, while the other Ni center acts as a Lewis acid, stabilizing the partial negative charges on the O atom of CO_2. This synergistic interaction significantly enhances the efficient conversion of CO_2 into CO. These findings underscore the promising potential of dual-metal synergistic catalysis in the field of electrochemical CO_2 reduction, establishing a new benchmark for deepening our understanding of the intricate structure-effect relationship (Fig. 7a).[124] Building upon this foundation, Lu's group made substantial progress in understanding the synergetic effects in dual-metal catalysts. In 2022, they systematically investigated three Ni_2 DACs, Ni_2–N_7, Ni_2–N_5C_2 and Ni_2–N_3C_4 with distinct coordination environments, identifying Ni_2–N_3C_4 as the most effective configuration for CO_2 reduction. The synergistic effect between the dual Ni centers in Ni_2–N_3C_4, enabled by the fine-tuning of its electronic structure, plays a pivotal role in optimizing the binding energies to the COOH* and CO* intermediates, leading to the superior electrocatalytic CO_2-to-CO reduction performance. This finding emphasizes the paramount importance of electronic structure modulation in the design of dual-atom catalysts (Fig. 7b).[125] Further advancements were made in 2023 with the synthesis of a uniform Ni_2-NCNT catalyst loaded on N-doped carbon nanotubes (NCNT), demonstrating an outstandingly high FE exceeding 90% for CO production across a wide range of potentials, accompanied by a significant partial current density for CO, which is much higher than that of single-atom catalyst Ni_1-NCNT. DFT calculations revealed that the synergistic interaction between the two Ni atoms in the Ni_2-NCNT configuration effectively stabilizes the *COOH intermediate and significantly reduces the free energy change in the rate-determining step when compared to the Ni_1- NCNT SAC, thereby enhancing CO_2 reduction efficiency (Fig. 7c and d).[126] The most recent achievement of Lu's group in 2024 involved strategic coordination environment optimization

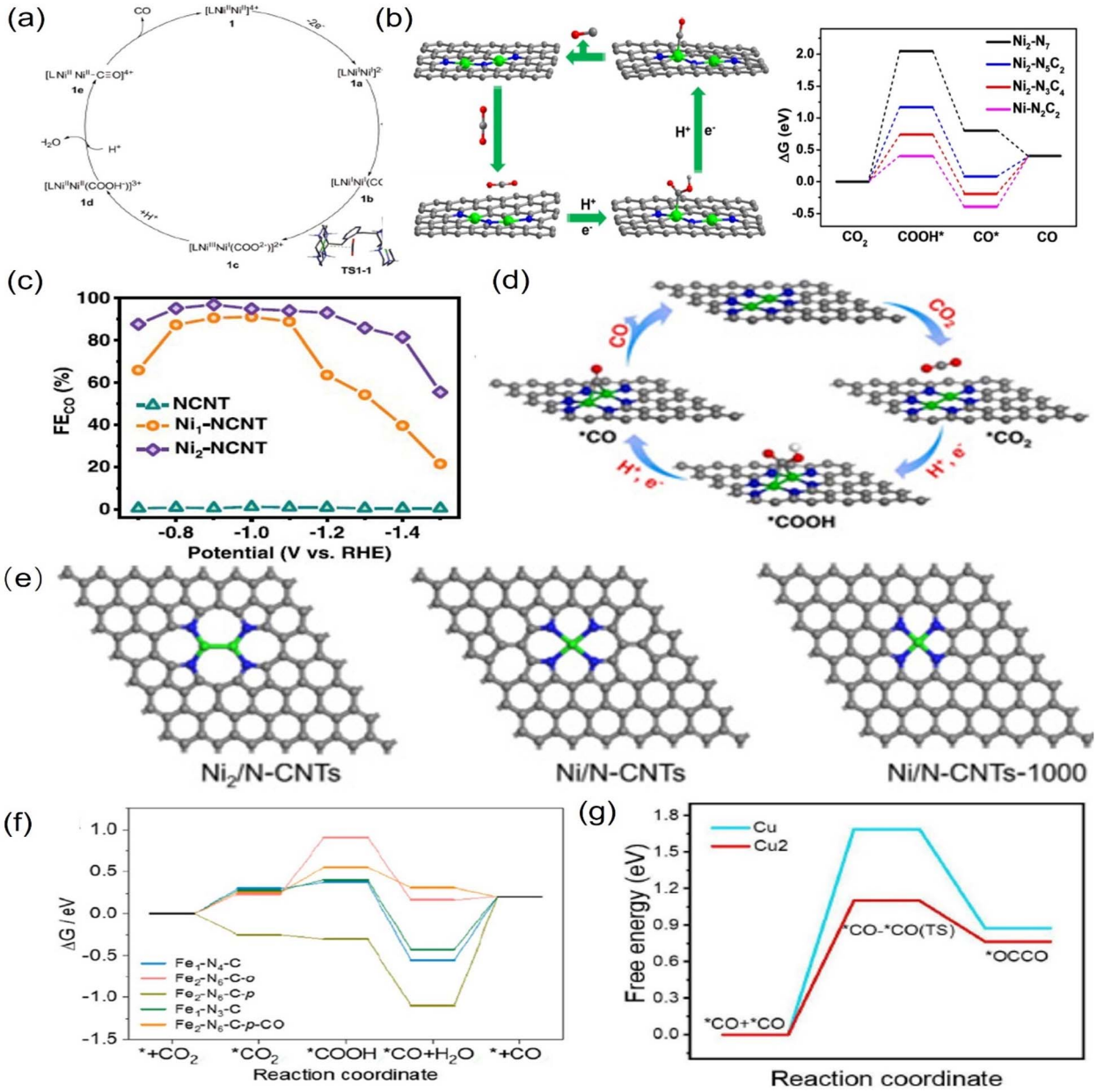

Fig. 7 (a) Mechanism for the conversion of CO_2 to CO, facilitated by a dinuclear nickel complex. (b) DFT calculations of $Ni_2N_3C_4$. (c) Faradaic efficiencies of CO for NCNT, Ni_1-NCNT and Ni_2-NCNT catalysts. (d) Pathways of Ni_2–N_3 (Ni_2-NCNT) for CO_2 electroreduction to CO. (e) The optimized structures of Ni_2/N-CNTs, Ni/N-CNTs, and Ni/N-CNTs-1000 (Ni_2/N-CNTs-1000). (f) The free energy diagram of the CO_2RR for Fe_1–N_4–C, Fe_2–N_6–C-o, Fe_2–N_6–C-p, Fe_1–N_3–C, and Fe_2–N_6–C-p-CO. (g) The energy barrier of Cu and Cu2. (a) Reproduced with permission.[124] Copyright 2017, the Royal Society of Chemistry. (b) Reproduced with permission.[125] Copyright 2022, John Wiley and Sons Ltd. (c and d) Reproduced with permission.[126] Copyright, 2023, Elsevier. (e) Reproduced with permission.[127] Copyright 2025, Springer. (f) Reproduced with permission.[128] Copyright 2022, American Chemical Society. (g) Reproduced with permission.[129] Copyright 2024, John Wiley and Sons Ltd.

of Ni_2 dual-atoms through pyrrolic-N modification. They discovered that the pyrrolic-N-coordinated Ni_2 catalysts showcase markedly enhanced electrocatalytic performance in the conversion of CO_2-to-CO, outperforming pyridinic-N-coordinated low-valent Ni catalysts. This significant advancement primarily stems from the fact that the intrinsically weak electron-donating characteristic of pyrrolic-N facilitates the formation of a reduced active site, which is extremely advantageous for the CO_2 electroreduction reaction. It was found that the reaction free energy pertaining to *COOH formation is notably lower on pyrrolic-N-coordinated Ni_2 catalysts in contrast to their pyridinic-N-coordinated Ni counterparts. Furthermore, the water molecules bound to the catalyst during the catalytic process are conducive to the formation of the key intermediate *COOH and the desorption of CO, which greatly enhances the catalytic efficiency (Fig. 7e).[127]

Advancements in dual-atom catalysts were notably achieved by Han, Lee, and their collaborators in the realm of iron-based

catalysis. They engineered dual-atom Fe_2 sites within the Fe_2–N_6–C catalyst, achieving a FE for CO production exceeding 80% over an extended range of applied potentials, in contrast to their single-atom Fe_1–N_4–C counterparts. The orbital coupling between the two adjacent Fe atoms in the Fe_2 sites facilitates electron delocalization and reduces the energy levels of the Fe-3d orbitals. This phenomenon enables charge transfer between the Fe atoms and the CO intermediate during *CO adsorption, thereby modulating the *CO binding energy and promoting CO desorption (Fig. 7f).[128] Another achievement was made by He, Wang *et al.*, who developed a novel copper-based metal–organic polyhedral dual-atom catalyst Cu2, featuring a Cu–Cu bond distance of 2.95 Å, which demonstrated unprecedented C_2H_4 production performance in 1.0 M KOH solution. The catalyst achieved a FE of 51% and a current density of 450 mA cm^{-2}, significantly outperforming both Cu single-atom catalysts and Cu nanoparticles. Mechanistic studies revealed that the unique Cu atom pairs in the catalyst can modulate *CO adsorption energy, promote C–C dimerization, and stabilize the *OCCO intermediate, thereby dramatically enhancing C_2H_4 production efficiency (Fig. 7g).[129]

These comprehensive studies have systematically elucidated the critical role of homonuclear dual-atom synergistic effects and coordination environment modulation in CO_2 electrocatalysis. The cooperative interaction between identical metal atoms optimizes reaction pathways, stabilizes key intermediates, and enhances catalytic performance in CO_2 reduction.

3.1.2 Hetero-dual atom synergistic catalysis. Heteronuclear dual-atom catalysts (DACs), composed of two distinct metal atoms, are a highly promising class of materials in the electrocatalytic CO_2RR due to their exceptional synergistic effects arising from unique electronic and geometric properties.[130] Many kinds of DACs like Ni–Ag, Cu–Co, Cu–Ni, Cu–Te and Ni–Co have been explored for the electrocatalytic CO_2RR. These catalysts mentioned above exhibit enhanced performance primarily through the electronic synergy includes charge transfer, polarization effects, and d-band center modulation. Heteronuclear DACs for the CO_2RR can be categorized into two types based on the distance between the two distinct metal centers: those with closely spaced metal atoms forming direct metal–metal (M–M) bonds, and those without significant M–M interactions. Through comprehensive experimental studies coupled with theoretical calculations, heteronuclear DACs have demonstrated significant potential for designing highly efficient and selective CO_2 reduction catalysts, offering critical support for achieving sustainable energy conversion and carbon neutrality goals. The presence of M–M bonds in heteronuclear DACs introduces unique electronic and geometric effects that profoundly influence their electrocatalytic CO_2RR performance. The formation of M–M bonds can facilitate orbital overlap leading to electron delocalization and modified d-band centers, which optimizes the adsorption strength of key intermediates like *COOH and *CO and lowers activation barriers for critical steps. Furthermore, in heteronuclear pairs, the electronegativity difference between metals induces charge asymmetry, where one metal acts as an electron donor (Lewis base) while the other serves as an electron acceptor (Lewis acid).[131] This cooperative effect enhances CO_2 activation by stabilizing charged intermediates. Han, Sun *et al.* reported Cu–Ni heteronuclear DACs with Cu–Ni bonds, which exhibited exceptional CO selectivity across all pH conditions, achieving a near-universal FE_{CO} of approximately 99% in acidic, neutral, and alkaline electrolytes. A particularly striking finding is the superior CO_2 utilization efficiency in acidic media (64.3%), which doubles the performance observed under alkaline conditions. Mechanistic investigations reveal strong electronic coupling between the Ni and Cu atomic sites, in which Cu acts as an electron donor to its neighboring Ni atom, leading to pronounced electron accumulation at Ni. Specifically, the Cu atoms induce an upward shift in the Ni d-band center position relative to the Fermi level, which thermodynamically favors and kinetically accelerates the critical *COOH intermediate formation step (Fig. 8a).[75] In another study, Wu, Chen and colleagues successfully developed CoCu heteronuclear DACs featuring direct Co–Cu bonding, achieving high-density Co–Cu atomic pairs with strong intermetallic interactions. DFT calculations show that the Co–Cu bond pushes the Co d-band center closer to the Fermi level, while the Cu d-band center remains deep. This tailored electronic structure balances intermediate adsorption strength, leading to industrial-scale current density for CO_2-to-CO conversion with high selectively. They discovered that the Co/Cu diatomic design synergistically addresses the limitations of single-atom catalysts by simultaneously lowering the energy barrier for *COOH formation, a challenge for Cu-SACs, while weakening *CO binding, a limitation of Co-SACs, thereby creating an optimized thermodynamic pathway (Fig. 8b and c).[132] Xu's group developed a Ni–Ag dual-atom catalyst (Ni–Ag/PC-N) with Ni–Ag bonded pairs supported on nitrogen-rich porous carbon, achieving an exceptional FE_{CO} exceeding 90% across a wide potential range, with a peak efficiency of 99.2%. This outstanding activity stems from the synergistic interplay between Ni and Ag atoms, mediated by their metal–metal bonding and electronic interactions, which modulate the d-band centers of both metals and optimize intermediate adsorption/desorption energetics. Mechanistic investigations demonstrated that in the Ni–Ag DACs, the Ni site lowers the energy barrier for the formation of the *COOH intermediate, whereas the Ag site alleviates catalyst poisoning induced by *CO adsorption, ultimately leading to a synergistic enhancement of performance.[133]

Recent advancements in hetero-DACs without M–M bonds have also revealed remarkable synergistic catalytic effects in CO_2 reduction, with multiple research teams developing high-performance catalysts through innovative design and synthesis strategies. Lu, Jiao, *et al.* reported a TeN_2–CuN_3 heteronuclear DAC with asymmetric coordination environments, offering a wide potential window for a high FE for CO production accompanied by enhanced reaction kinetics. It was confirmed that the Te center facilitates the activation of CO_2, while the Cu center aids in the dissociation of H_2O. Both experimental and theoretical findings indicate that the TeN_2–CuN_3 configuration can collaboratively reduce the energy barriers associated with the rate-limiting step, thereby enhancing proton transfer kinetics (Fig. 8d).[40] In another

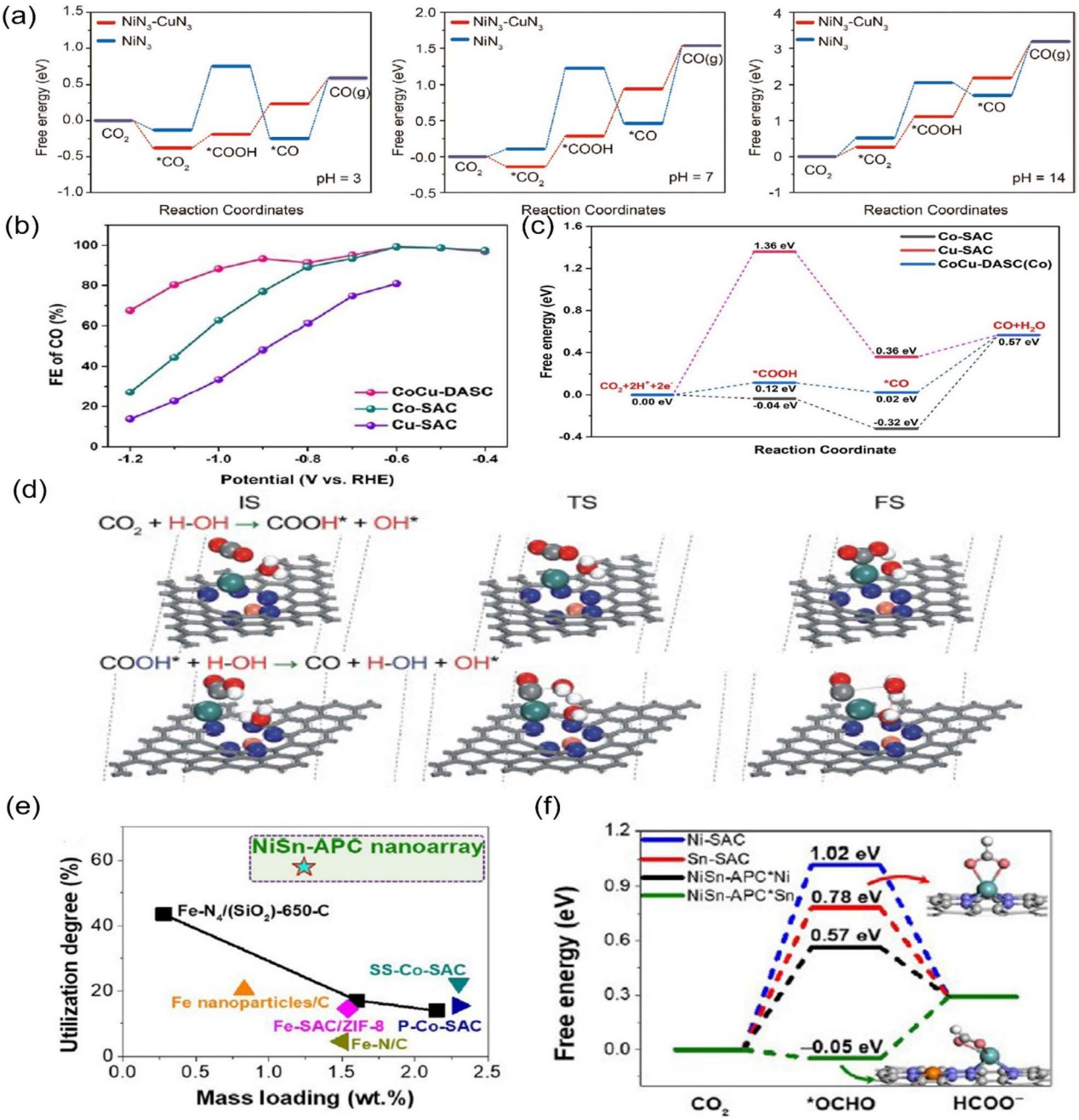

Fig. 8 (a) DFT calculations of NiN_3–CuN_3 and NiN_3. (b) faradaic efficiencies of CO measured in a H-type cell. (c) Free energy profiles of the CO_2RR on CoCu-DASC Co-SAC and Cu-SAC. (d) Calculated configurations for the conversions of CO_2 → COOH* and COOH* → CO (IS, initial state; TS, transition state; FS, final state) over TeN_2–CuN_3 DAC. (e) A comparative study on the utilization degree of various materials. (f) Free energy diagrams of the CO_2RR for production of formate. (a) Reproduced with permission.[75] Copyright 2023, Wiley. (b and c) Reproduced with permission.[132] Copyright 2022, John Wiley and Sons Ltd. (d) Reproduced with permission.[40] Copyright, 2023, Springer Nature. (e and f) Reproduced with permission.[134] Copyright 2021, John Wiley and Sons Ltd.

example, Wei, Shao, *et al.* constructed a NiSn DAC featuring adjacent Ni and Sn atoms, each bonded to four nitrogen atoms, forming a N_4–Ni–Sn–N_4 configuration. The fabricated NiSn DAC showcased exceptional efficiency in the conversion of CO_2 to formate *via* the CO_2RR, attaining a remarkable TOF of 4752 h^{-1}. It was found that the neighboring Ni–N_4 configuration could facilitate electron redistribution within the Sn atom, with the synergistic catalytic effect leading to the lowered energy barrier for *OCHO key intermediate formation (Fig. 8e and f).[134]

In summary, recent advancements in heteronuclear DACs for CO_2 reduction have demonstrated significant potential in achieving high efficiency and selectivity. Both DACs with M–M bonds and those without exhibit remarkable synergistic effects, which are primarily attributed to their unique electronic

configurations. The presence of M–M bonds facilitates orbital overlap, electron delocalization, and modified d-band centers, optimizing the adsorption strength of key intermediates and lowering activation barriers. In contrast, DACs without M–M bonds often rely on asymmetric coordination environments or specific atomic pairings to enhance catalytic performance.

3.2 Dual-metal nanoparticle synergistic catalysis for the electrocatalytic CO_2RR

Copper is widely regarded as one of the most promising candidates for the electrocatalytic CO_2RR due to its suitable adsorption capacity for reaction intermediates. However, the performance of Cu-based catalysts is often limited by issues such as poor selectivity, low activity, and rapid deactivation. These challenges necessitate the development of advanced strategies to enhance their catalytic performance. One effective strategy to overcome these limitations involves modifying copper-based nanoparticle catalysts by incorporating a secondary metal into the system. The electronic coupling between Cu and the secondary metal can modulate the electronic density of states, facilitating the charge transfer between the catalyst and reactants.[135] Most importantly, this approach can generate dual-active sites, creating a synergistic catalytic effect that enhances the overall catalytic performance.

In this section, the main focus is on leveraging the synergistic effects between the copper host and guest metals to tune the electronic and geometric structures of the resulting nanoparticle catalysts. By modifying the dual-active sites, the catalytic performance can be significantly improved. A wide range of guest metals, encompassing main-group metals, non-precious transition metals, noble metals, and lanthanides, will be extensively studied as secondary metals incorporated into Cu-based catalysts to explore their potential for enhancing the product efficiency of the CO_2RR. A particular focus will be placed on elucidating the mechanisms underlying synergetic catalysis in the context of the CO_2RR. Understanding these cooperative mechanisms holds immense significance to elucidate the structure–activity relationships and identify the key factors that govern their catalytic performance.

3.2.1 Copper and main group metals. Main-group metal elements, such as tin (Sn), bismuth (Bi), aluminum (Al), gallium (Ga), and indium (In), offer unique opportunities for modulating the electronic and geometric properties of copper-based nanomaterials. When main group metal elements are doped into copper, the p-electrons of the main group metal elements can hybridize with the d-electrons of copper. This hybridization leads to changes in the energy levels and distribution of electrons in the catalyst. In recent years, substantial progress has been achieved in the field of research focused on integrating main group metals into copper-based catalysts for the CO_2RR. In this context, the incorporation of main group metals has been pivotal in optimizing catalytic performance for the production of C_1 and C_2 compounds. When incorporated into copper catalysts, these elements can induce lattice strain, alter the electronic density of states, and create new active sites. For instance, some main group metals like Bi can highly inhibit the competing HER, and thus greatly enhance CO_2 reduction, while Al doping can introduce electron-deficient regions near the copper surface, enhancing the adsorption of CO_2 and facilitating its activation. This, in turn, can lead to improved CO_2 reduction efficiency and selectivity towards desired products. Additionally, the presence of main-group metals can stabilize the copper nanostructures, preventing aggregation and enhancing their long-term stability during electrocatalytic reactions.[136]

The introduction of main-group elements can enhance the control of copper-based catalysts over the electrochemical CO_2RR for selective generation of C_1 products. For example, Pan *et al.* electrochemically deposited the main group metal indium (In) onto CuCl-decorated copper foil, successfully constructing a Cu–$CuInO_2$ dual-metal material with a stable Cu^0/Cu^+ state. It was found that the high HER overpotential of In could minimize parasitic H_2 production, directing more electrons to CO_2 reduction, which enabled $CuInO_2$ catalysts to achieve FE_{HER} < 15% and FE_{CO} of 89% at −0.9 V *vs.* RHE. The $CuInO_2$ catalyst demonstrated unique synergistic effects through electronic structure modulation, wherein p-orbitals of In hybridize with d-orbitals of Cu to redistribute charge density, optimize *CO binding energy, weaken *CO adsorption, and strengthen *COOH stabilization, thereby favoring CO production over C_2 pathways (Fig. 9a).[137] Numerous investigations have demonstrated that incorporating main group elements into copper-based catalysts can substantially enhance the catalytic pathway by lowering the energy barrier for C–C coupling, thereby promoting the formation of C_2 products. For example, Wang, Jiang *et al.* reported the construction of a CuO/SnO_2 dual-metal heterostructure through *in situ* electrochemical evolution, successfully regulating the C_1/C_2 product selectivity through the introduction of Sn. Most importantly, Sn^{2+}/Sn^0 in Cu/SnO_{2-x} (oxygen-deficient SnO_2) can stabilize *COOH and *CHOCO intermediates, thereby facilitating C–C coupling for CH_3CH_2OH production. Through strong d-p orbital hybridization between Cu (3d) and SnO_{2-x} (O2p), key intermediates are synergistically stabilized, leading to a lowered energy barrier for C_2 product formation. Besides, the introduction of Sn promoted the synergistic adsorption of *COOH and *CHOCO intermediates at the Cu/SnO_{2-x} interface, significantly enhancing ethanol production efficiency (Fig. 9b).[138] Meanwhile, Zhang's group introduced the main group metal Bi to prepare a single-atom Bi-modified Cu alloy (BiCu-SAA) for the first time. The high HER overpotential of Bi effectively suppresses competing reactions, while single-atom Bi doping modulates the electronic structure of Cu to stabilize *CO intermediates and facilitate efficient C–C coupling. Through this synergistic Bi–Cu interaction, the BiCu-SAA catalyst achieves exceptional performance at industrial current densities (400 mA cm^{-2}), delivering a remarkable 73.4% FE for C_{2+} products (Fig. 9c and d).[139] In another study, Wang *et al.* incorporated the main-group metal gallium (Ga) into a catalyst system, creating a dual-metal catalyst by combining it with copper (Cu). The resulting CuGa catalyst demonstrated a cathodic energy efficiency (EE) exceeding 50% for C_{2+} products at a current density of 1 A cm^{-2}, significantly surpassing the performance of pure Cu, which exhibited an EE of

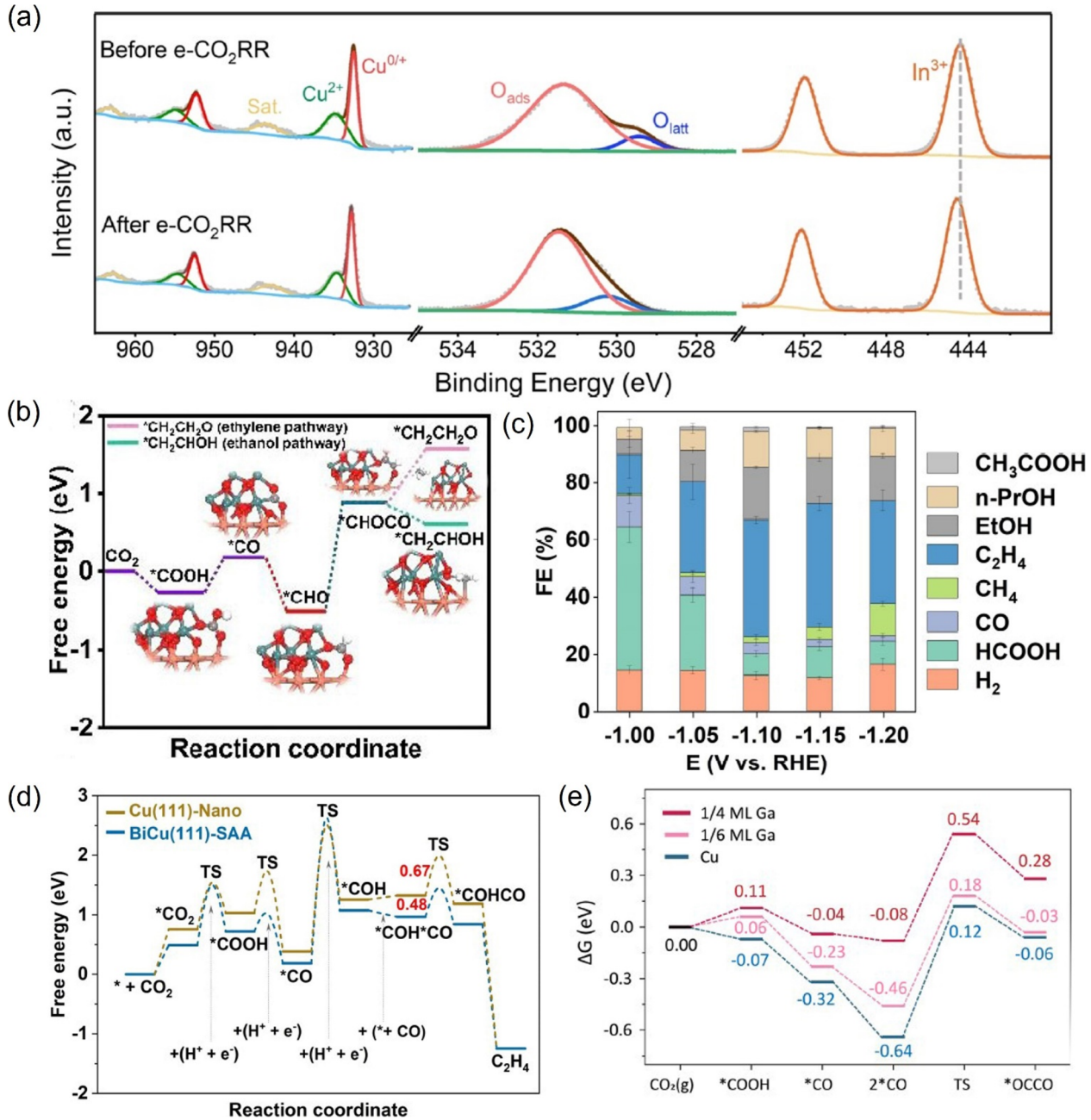

Fig. 9 (a) XPS spectra of Cu–In-120 s before and after the e-CO_2RR. (b) The comparison of free energy for the ethylene and ethanol pathways on Cu/SnO_{2-x}. (c) FE values of various products on the BiCu-SAA at different applied potentials in an H-type cell. (d) The free energy diagram for the CO_2RR to C_2H_4 on the BiCu(111)-SAA and Cu(111)-Nano. (e) The free energy surface for CO_2 reduction to CO and CO–CO coupling with the Cu (100) surface with 0, 1/6, and 1/4 ML of Ga. (a) Reproduced with permission.[137] Copyright 2023, American Chemical Society. (b) Reproduced with permission.[138] Copyright 2023, John Wiley and Sons Ltd. (c and d) Reproduced with permission.[139] Copyright, 2023, John Wiley and Sons Ltd. (e) Reproduced with permission.[140] Copyright 2024, Springer Nature.

approximately 30%. They discovered that Ga, with its lower electronegativity than Cu, can donate electrons to Cu, increasing the occupancy of Cu's sp-band, which strengthened σ-repulsion between Cu and adsorbed CO (*CO), weakening *CO binding energy. Besides, Ga can stabilize Cu^+ states under ambient conditions, which may facilitate *CO adsorption and C–C coupling, leading to the high performance for C_{2+} production (Fig. 9e).[140]

In summary, the incorporation of main-group metals into copper-based catalysts offers a powerful strategy to optimize CO_2 electroreduction by modulating electronic and geometric properties. These elements enhance selectivity and efficiency—either by suppressing the HER, stabilizing key intermediates, or lowering C–C coupling barriers—enabling high-performance C_1 or C_{2+} production.

3.2.2 Copper and non-precious transition metals. Non-precious transition metals, such as iron (Fe), cobalt (Co), nickel (Ni), and zinc (Zn) are attractive dopants for copper-based nanomaterials due to their abundance, low cost, and potential to enhance catalytic activity. These metals can form alloys or intermetallic compounds with copper, leading to synergistic effects that improve CO_2 adsorption and reduction kinetics. The d-electron configuration of transition metals plays a crucial role in determining their catalytic properties. When a non-noble transition metal atom, such as Co, substitutes a copper atom in a Cu-based catalyst, it induces a drastic change in the density of states (DOS).[141] Moreover, when a non-noble transition metal with a different electronegativity is introduced into the copper lattice, it can lead to bond polarization. This polarization affects the distribution of electron density around the active sites, influencing the adsorption and activation of CO_2 molecules.[142] The d-electron interactions and electronegativity differences between the dopant atoms and copper play crucial roles in determining the catalytic pathway and efficiency for the CO_2RR. Furthermore, the presence of non-precious transition metals can modulate the surface energy and reactivity of copper, enabling the tuning of product selectivity and reaction rates.[143]

Many previous studies have shown that non-precious transition metals, owing to their distinctive d-electron configurations, can modulate the electronic structure and surface properties of Cu catalysts. Streb *et al.* developed a CuCo dual-metal electrocatalyst, formed under reaction conditions that drive Cu sites from single-atom states into small Cu clusters (Cu^0) while maintaining Co sites in a monodispersed state, which enabled highly selective CO_2-to-EtOH conversion with a FE > 70%. It was discovered that a synergistic CO spillover mechanism occurred where Co sites efficiently generated CO and created a high local CO concentration, while Cu sites received this CO and facilitate C–C coupling to produce EtOH, thereby significantly enhancing C_2 product selectivity by reducing the CO transport distance. The close proximity of Co and Cu sites enables efficient CO_2-to-ethanol conversion through the CO spillover mechanism, while inhibiting side reactions, demonstrating the importance of dual-metal catalysts in designing efficient CO_2 reduction systems (Fig. 10a).[59] In another study, Ma, Zhang, *et al.* added a trace amount of Ni to the surface of CuO nanosheets which markedly improved both the stability and FE for the electrochemical reduction of CO_2 into C_2 products. Ni doping into CuO nanosheets could significantly inhibit the dissolution of Cu during the CO_2RR by strengthening the bonds between surface and subsurface Cu atoms. Hence, unlike pure CuO, which is prone to transforming into dendritic structures during prolonged reactions, the CuO + Ni-surface dual-metal system maintains its nanosheet architecture, ensuring consistent and reliable catalytic performance over time. DFT calculations and *operando* ATR-SEIRAS revealed that Ni-doped CuO surfaces exhibited stronger *CO adsorption and lower energy barriers for *CO dimerization, promoting C–C coupling, offering a cost-effective synergistic strategy to enhance CO_2RR efficiency and durability for C_2 production (Fig. 10b and c).[62] The non-precious transition metal Zn is rich with d electrons. Schuhmann *et al.* doped the Cu-based catalyst with Zn to obtain the dual-metal gas diffusion electrodes (GDEs) B–Cu–Zn, which can enhance the electrocatalytic CO_2RR activity toward multi-carbon C_{2+} products with high stability. *Operando* Raman spectroscopy confirmed that Zn incorporation helps retain Cu^+ species under reduction conditions, which can suppress the HER and facilitate C–C coupling, while the Cu^+ sites could lower the energy barrier for *OCCO intermediate formation, the key step in C_{2+} production. The synergistic interplay between Cu and Zn in B–Cu–Zn GDEs significantly improved the CO_2RR performance mainly through the stabilization of Cu^+ species by Zn and dynamic protection of active site Cu through Zn sacrificial oxidation (Fig. 10d and e).[60]

In summary, the incorporation of non-precious transition metals into Cu-based catalysts introduces synergistic effects that significantly enhance CO_2 electroreduction toward C_{2+} products. These dopants modify the electronic structure of Cu through their distinct d-electron configurations and electronegativity differences, optimizing CO_2 adsorption, stabilizing key intermediates like *CO and *OCCO, and lowering energy barriers for C–C coupling. Studies on CuCo, CuNi, and CuZn nanoparticle systems demonstrate that dual-metal interactions—such as CO spillover, strengthened Cu surface bonding, and sacrificial stabilization of Cu^+—play pivotal roles in improving selectivity and durability at high current densities.[61] These findings highlight the potential of cost-effective dual-metal catalysts to advance the CO_2RR by precisely tuning electronic and geometric properties, offering a scalable pathway for sustainable C_{2+} production.

3.2.3 Copper and precious transition metals. Noble metals, such as silver (Ag), gold (Au), and palladium (Pd), are well-known for their exceptional catalytic properties and are often used as dopants to enhance the performance of copper-based nanomaterials in CO_2 reduction. These metals can act as co-catalysts, promoting the activation of CO_2 and facilitating the formation of key reaction intermediates. For instance, Ag doping has been reported to increase the FE of copper-based catalysts towards ethylene production, owing to the ability of Ag to stabilize the *CO intermediate and promote its subsequent dimerization.[144] Similarly, Au doping can enhance the selectivity towards multi-carbon products by modulating the adsorption energy of reaction intermediates on the copper surface. However, the high cost of noble metals necessitates the development of strategies for their efficient utilization and recycling.[145]

Compared to other noble metals like Au, Pd, and Pt for doping Cu-based CO_2RR catalysts, Ag presents distinct and superior advantages, particularly in terms of cost-effectiveness. Moreover, Ag demonstrates weaker *CO adsorption compared to Cu but stronger adsorption than Au, thereby establishing an optimal intermediate state conducive to C–C coupling. For example, Wang, Ye, *et al.* developed a Ag-doped Cu_2O–Cu catalyst, Ag/Cu_2O–Cu, which can significantly enhance CO_2 electroreduction CO_2 to multi-carbon C_{2+} products at an industrial current density of 1.0 A cm^{-2} with a FE of 76.5%. *Operando* Raman spectroscopy and XPS analyses confirmed that Ag incorporation effectively stabilizes metastable Cu^+ species

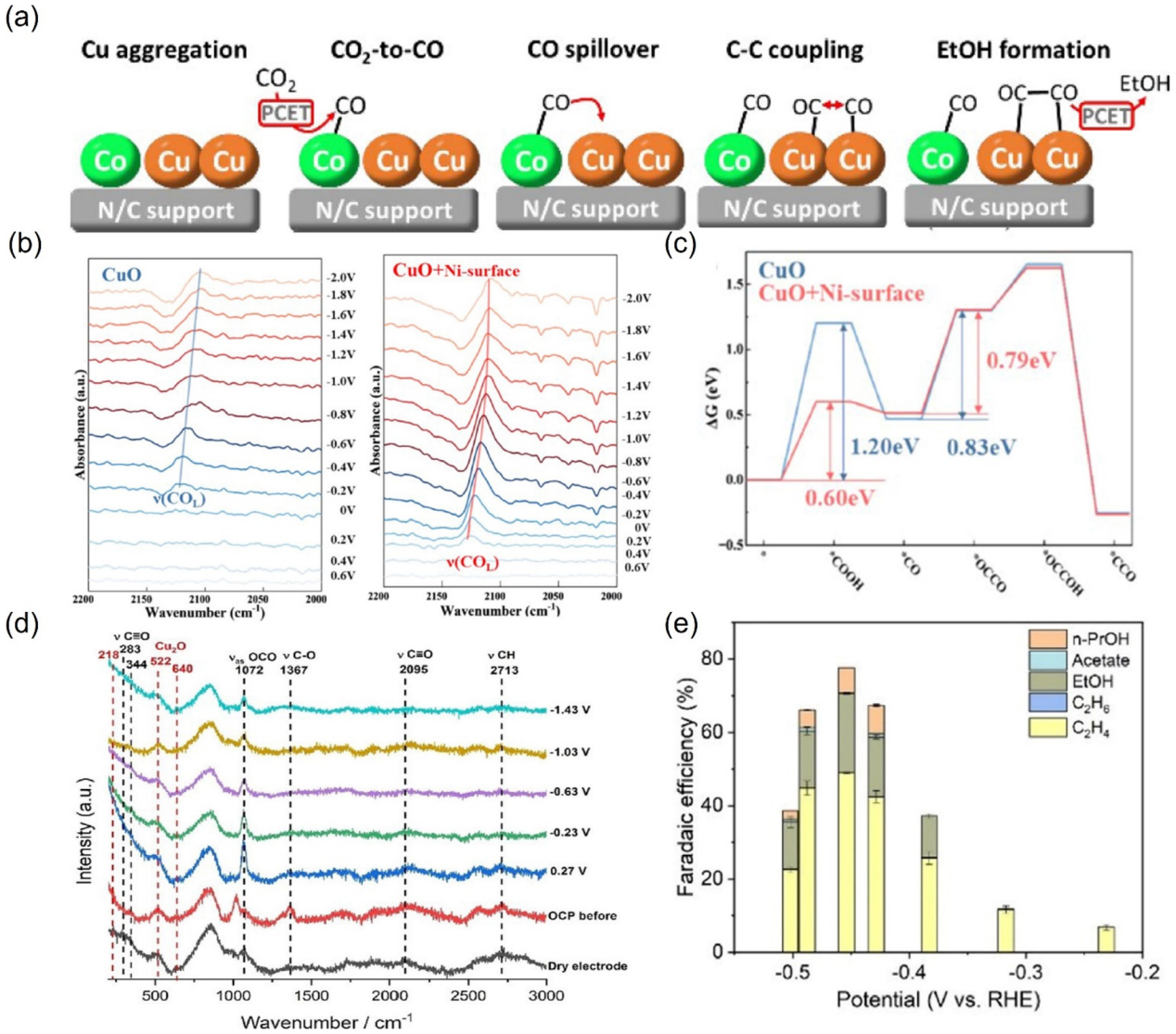

Fig. 10 (a) The CO spillover mechanism for efficient ethanol formation at the CoCu electrocatalyst. (b) FT-IR characterization of CuO and the CuO + Ni-surface. (c) Relative Gibbs free energy diagrams for the CO_2RR. (d) *Operando* electrochemical Raman spectra for the 0.5B–Cu : 0.025Zn GDE. (e) Faradaic efficiencies for CO_2RR products at a catalyst loading of 0.5 mg cm^{-2} B–Cu at different potentials. (a) Reproduced with permission.[59] Copyright 2024, American Chemical Society. (b and c) Reproduced with permission.[62] Copyright 2025, Elsevier. (d and e) Reproduced with permission.[60] Copyright 2021, John Wiley and Sons Ltd.

(Cu_2O) under reducing conditions, maintaining robust $Ag/Cu^+/Cu^0$ interfaces during the CO_2RR, which is a critical feature for facilitating C–C coupling. The intermediate *CO binding strength of Ag (between Cu and Au) creates a synergistic system, where efficient *CO production couples with facile spillover to Cu^+/Cu^0 sites, lowering the *OCCO formation barrier by 56% *versus* Cu_2O and dramatically boosting C_{2+} selectivity (Fig. 11a and b).[144] Li's research group also developed a Ag-doped Cu-based material featuring (111)-facet-exposed Cu nanosheets decorated with Ag nanoparticles. This composite demonstrated remarkable efficiency in electrochemically converting CO_2 to ethanol, achieving a FE of 56.5 ± 2.6% and a partial current density of 356.7 ± 9.5 mA cm^{-2}. They discovered that the synergistic effect between Ag and Cu in the dual-metal catalyst lies in Ag's ability to supply CO to Cu(111) facets—which efficiently generate $*CH_2$ intermediates—promoting asymmetric $*CH_2$–CO coupling for ethanol production, while suppressing excessive *CO hydrogenation to methane (FE drops from 27.3% on bare Cu to 3.7%) and shifting selectivity away from symmetric CO–CO coupling that favors ethanol production. This dynamic interplay, enhanced by the layered Cu/Ag structure, optimizes local CO coverage and intermediate utilization, steering selectivity toward ethanol over hydrocarbons (Fig. 11c and d).[146]

Many significant studies have highlighted the promotional role of doping other precious metals, such as Pd and Au, into Cu-based nanomaterials in facilitating the electrocatalytic reduction of CO_2. For example, Yang, Che, *et al.* reported two platinum-group-metal doped Cu-based dual-metal catalysts Pd_1Cu and Pt_1Cu for the electrocatalytic CO_2RR. It was found

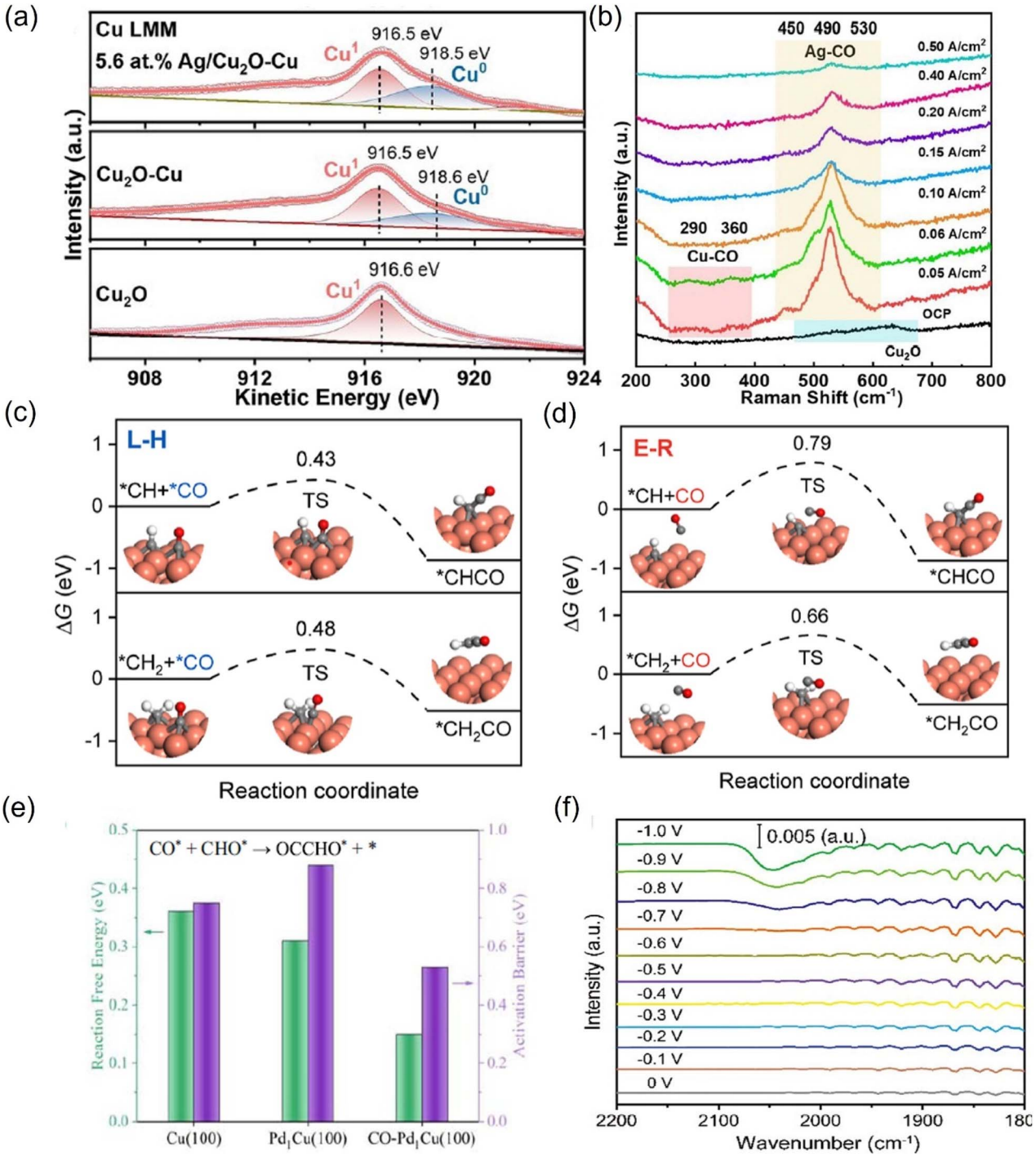

Fig. 11 (a) Cu LMM spectra of Cu_2O, Cu_2O–Cu, and 5.6 atom% Ag/Cu_2O–Cu catalysts. (b) Raman shift of the 5.6 atom% Ag/Cu_2O–Cu catalyst. DFT calculations: barriers for $*CH_x$ ($x = 1, 2$) coupling with *CO/CO *via* (c) L–H and (d) E–R mechanisms. (e) The reaction free energies and activation barriers of C–C coupling on Cu (100) and Pd_1Cu (100). (f) *In situ* ATR-IR spectra of Au–Cu Janus NSs. (a and b) Reproduced with permission.[144] Copyright 2025, American Chemical Society. (c and d) Reproduced with permission.[146] Copyright 2024, American Chemical Society. (e) Reproduced with permission.[147] Copyright 2023, Springer Nature. (f) Reproduced with permission.[148] Copyright 2022, Wiley-VCH Verlag.

that both Pt and Pd single-atom dopants boost CO* adsorption on Cu, serving as CO* reservoirs that balance coverage and prevent poisoning, thereby enhancing C–C coupling for hydrocarbon production. In addition, Pt and Pd single-atom doping in Cu synergistically enhances the CO_2RR by enriching CO* coverage while suppressing the HER and preserving facet-dependent selectivity (CH_4 on Cu (111) and C_2H_4 on Cu (100)). Meanwhile, Pd_1Cu demonstrates superior performance (CH_4:

25%; C_2H_4: 33%) by optimally balancing CO* stabilization and hydrogenation kinetics compared to Pt_1Cu (Fig. 11e).[147] Huang *et al.* reported gold–copper (Au–Cu) Janus nanostructures as a dual-metal catalyst capable of efficiently electroreducing CO_2 to C_{2+} products, achieving a C_{2+} selectivity of 67%. *In situ* ATR-IR spectroscopy revealed that the Au–Cu synergy enables selective CO_2-to-CO* conversion at Au sites (the critical intermediate for C–C coupling) *via* weak CO* binding, while adjacent Cu sites facilitate CO* hydrogenation to hydrocarbons and C–C coupling. The enhanced CO* coverage on Au–Cu Janus nanostructures compared to pure Cu can be attributed to CO* spillover from Au to Cu domains. They discovered that fine-tuning Au–Cu interfaces of Janus structures could enhance selectivity toward C_{2+} products, which outperformed the physical mixtures or core–shell structures in the CO_2RR, offering a general strategy for multi-step reaction catalysts (Fig. 11f).[148]

In summary, doping noble metals like Ag, Pd, and Au into Cu-based nanomaterials significantly enhances their performance in CO_2 electroreduction.[149] Ag stands out for its cost-effectiveness and optimal CO adsorption strength, facilitating C–C coupling and boosting C_{2+} selectivity. Pd and Au doping also promote CO adsorption and balance coverage, preventing poisoning and enhancing C–C coupling for hydrocarbon production.[150] These findings underscore the critical role of precious transition metal doped Cu-based dual-metal synergies in modulating intermediate adsorption energies, stabilizing reactive species, and steering selectivity toward high-value C_{2+} products.

3.2.4 Copper and lanthanide metals. Lanthanide metal elements, such as cerium (Ce), lanthanum (La), gadolinium (Gd) and neodymium (Nd) possess unique electronic properties that can be harnessed to enhance the performance of copper-based nanomaterials in CO_2 reduction.[151,152] The unique f-orbital electrons of lanthanide metal elements significantly influence their doping effects in copper-based nanomaterials for electrocatalytic CO_2 reduction.[135,153]

The incorporation of lanthanides into copper-based catalysts introduces lattice strain due to the substantial difference in ionic radii between lanthanides and copper.[149,154,155] This strain can modulate the electronic structure and binding energies of reaction intermediates, thereby lowering the activation energy barriers and optimizing the reaction pathway for CO_2 reduction.[156] Han, Sun, *et al.* reported that the atomic doping of Gd into CuO_x catalysts (Gd_1/CuO_x) induces tensile strain and stabilizes Cu^+ species, enabling an exceptional FE of 81.4% for C_{2+} products with a partial current density of 444.3 mA cm^{-2} at -0.8 V *vs.* RHE, demonstrating its high efficiency in the CO_2RR. They discovered that the unique 4f electron configuration and unfilled 5d orbitals of Gd can enhance spin–orbit coupling, modifying the local electron density around Cu atoms and inhibiting their reduction to Cu^0. This Gd–Cu synergy facilitated efficient electron transfer during the CO_2RR, significantly improving reaction kinetics. Additionally, the tensile strain induced through the large ionic radius of Gd introduced into the CuO_x lattice could optimize the d-band center of Cu and fine-tune the binding energy of key intermediates *CO. This strain effect further reduces the Gibbs free energy barrier for the C–C coupling step ($2CO \rightarrow O^*CCO$), thereby promoting the selective formation of C_{2+} products (Fig. 12a and b).[157] Liang *et al.* constructed a Cu/CeO_2 dual-metal catalyst, in which the larger lattice spacing of the CeO_2 (111) plane compared to Cu_2O stretches Cu–O bonds, introducing tensile strain in the Cu domains. It was discovered that the tensile strain in the Cu/CeO_2 heterostructure upshifted the d-band center of Cu, which can enhance *CO adsorption and promote dimerization, facilitating C–C coupling for multicarbon formation. DFT calculations revealed that the synergistic Cu and CeO_2 interaction drives charge transfer from Cu to CeO_2, creating electron-deficient interfacial Cu sites. By combining tensile strain and electron deficiency, Cu and CeO_2 synergistically optimize CO coverage and stabilize key intermediates, collectively boosting selectivity toward C_{2+} products (Fig. 12c and d).[158]

Additionally, the unique electronic configurations of lanthanides can also regulate the electronic structure of active sites or modulate the d-band center of copper, enhancing *CO adsorption and stabilizing Cu^+ sites critical for multicarbon product formation. Han, Zhu, *et al.* developed a Pr–Cu dual-metal oxide heterointerface, specifically Pr_6O_{11}–Cu-SS, which efficiently catalyzes the CO_2RR to C_{2+} products, achieving a high FE of 71.3% for C_{2+} alcohols (ethanol and *n*-propanol) at a current density of 700 mA cm^{-2}. It was found that Pr doping in Cu oxides could generate an oxygen vacancy (O_{vac})-rich interface, which modulated the electronic structure of Cu ($Cu^{\delta+}/Cu^0$) to enhance CO adsorption and asymmetric C–C coupling. The Pr–O–Cu linkages further stabilized key intermediates, enabling sustained high activity and stability even at industrial current densities. DFT calculations and *in situ* Raman spectroscopy revealed that the Pr–Cu interface induced mixed *CO adsorption configurations, in which this asymmetry promoted C_{2+} alcohol formation over ethylene by stabilizing $*OCHCH_3$ intermediates (Fig. 12e).[159] In another study, Han, Sun, *et al.* developed a La-doped Cu electrocatalyst that achieved a remarkable FE of 86.2% for C_{2+} products at a partial current density of -775.8 mA cm^{-2} in acidic electrolyte during CO_2 reduction. As validated by *in situ* SERS detection, owing to the synergistic effects of La and Cu, the mesoporous channels in La–Cu hollow spheres (La–Cu HS) could concentrate K^+ and OH^- near the catalyst surface, creating a localized alkaline microenvironment that can suppress the HER and promote C–C coupling. Electronic structure analysis reveals that due to the difference in electronegativity, La can donate electrons to Cu, which enhances *CO stabilization. DFT calculations further confirm that the resulting La–O–Cu linkages could stabilize metallic Cu during the CO_2RR, while enabling synergistic catalysis, where La promoted CO generation and lowered C–C coupling barriers, while Cu maintained conductive pathways and active sites for CO_2 reduction.[160]

In summary, the integration of lanthanide metals into copper-based nanomaterials presents a promising strategy for enhancing CO_2 reduction performance. By leveraging the unique electronic properties of lanthanides, such as their f-orbital electrons and specific electron configurations, researchers have been able to modulate the reaction pathways of copper-based catalysts.[158] The synergistic interactions between copper and lanthanides, driven by factors such as

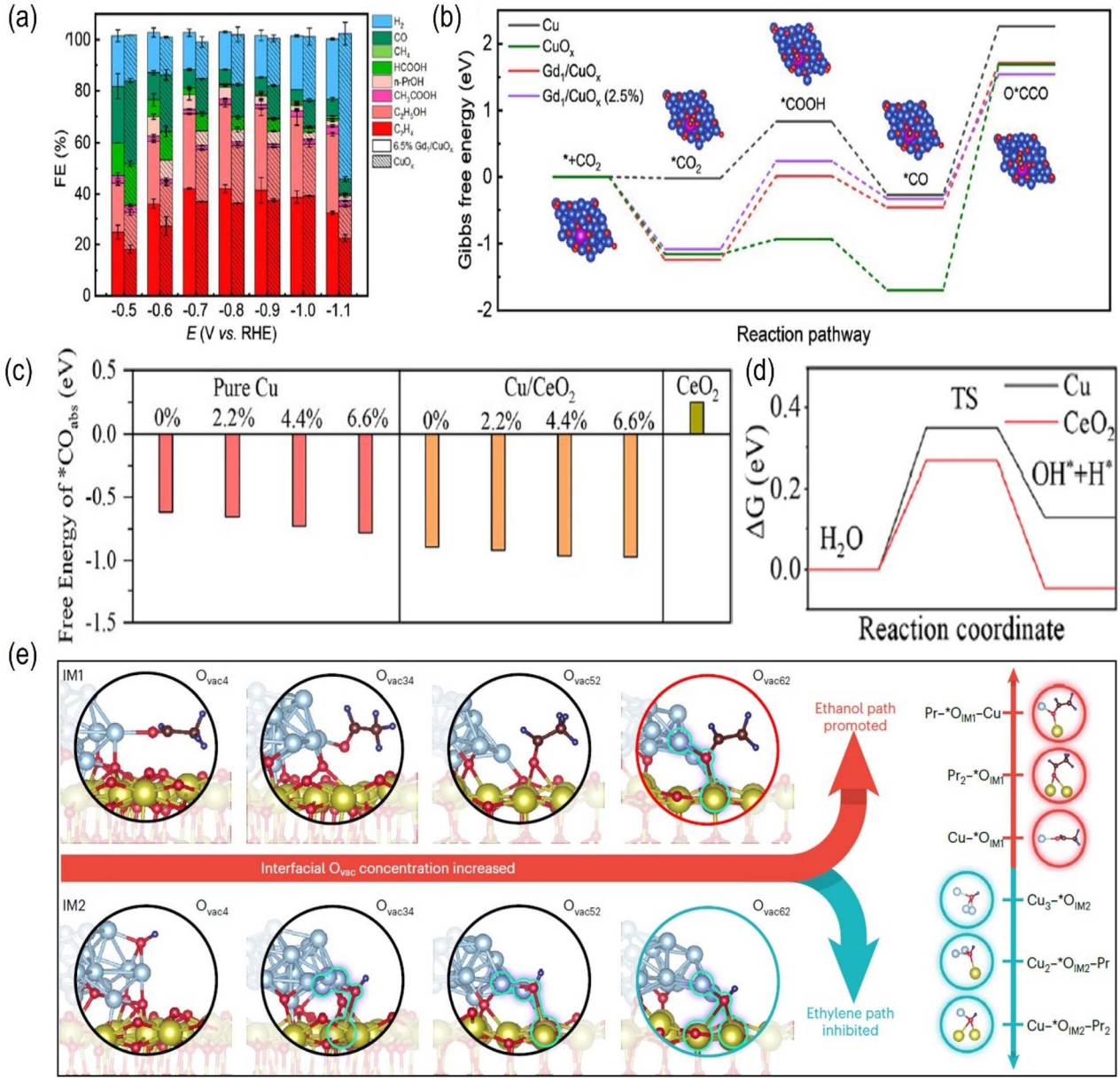

Fig. 12 (a) Faradaic efficiencies for CO_2RR products on 6.5% Gd_1/CuO_x and CuO_x. (b) The free energy diagram of the CO_2RR for Cu, CuO_x, Gd_1/CuO_x, and Gd_1/CuO_x (2.5%). (c) Calculated *CO adsorption energies on standard Cu, stretched Cu, Cu/CeO_2, the stretched Cu/CeO_2 interface, and CeO_2. (d) The transition barrier investigation for H_2O dissociation on Cu (111) and CeO_2 (111). (e) Adsorption configurations of different Pr_6O_{11}-O_{vac}–Cu models. (a and b) Reproduced with permission.[157] Copyright 2023, American Chemical Society. (c and d) Reproduced with permission.[158] Copyright 2023, American Chemical Society. (e) Reproduced with permission.[159] Copyright, 2025, Springer Nature.

lattice strain, electron transfer, and interface engineering, have opened up new avenues for the development of highly efficient electrocatalysts for the CO_2RR.[161]

4 Conclusions

The development of dual-metal synergistic catalysts has emerged as a powerful strategy to enhance the efficiency, selectivity, and stability of the electrocatalytic CO_2RR. This review systematically explores the design principles, mechanistic insights, and catalytic performance of dual-metal catalysts, emphasizing the critical role of synergistic effects of different metal centers in optimizing CO_2RR pathways, and elucidating the structure–activity correlations. Leveraging the unique synergistic effects of two metal centers has led to remarkable progress in tailoring catalyst properties to favor desired reaction intermediates and suppress competing HER.

This review first focuses the design principles of dual-metal catalysts with synergistic effects for the CO_2RR, focusing on electronic and geometric structure regulation. Electronic structure regulation involves chemical state, vacancy, and coordination environment modifications, while geometric structure regulation

encompasses crystal facet, nanoparticle size, and morphology adjustments. These strategies are crucial for optimizing the adsorption and activation of reactants, stabilizing intermediate states, and refining the catalytic pathway. Next, the review delves into the influence of different types of dual-metal active sites, including dual-atom metal catalysts (DACs) and dual-metal nanomaterial catalysts. DACs are characterized by their atomic efficiency and precise electronic structures, while dual-metal nanomaterial catalysts offer more complex surface architectures and synergistic effects at the nanoscale. For dual-metal nanomaterial catalysts, various secondary metals, such as main-group metals, non-precious transition metals, noble metals and lanthanides, are studied for their potential to enhance copper-based catalysts for CO_2RR performance. The review mainly explores various dual-metal catalysts with synergistic catalytic effects, highlighting their distinct advantages and mechanisms for promoting the CO_2RR. The review also underscores the importance of rational design and innovative synthesis strategies in developing advanced CO_2RR electrocatalysts.

Despite the significant progress made in dual-metal catalysis for the CO_2RR, several challenges remain. Future research should focus on the following areas: (1) enhanced catalytic stability: improving the long-term stability of dual-metal catalysts is crucial for their practical application. Strategies such as surface passivation, defect engineering, and support optimization could be explored to mitigate deactivation pathways. (2) Developing scalable and cost-effective production methods for dual-metal catalysts is essential for their commercialization. Research on continuous flow reactors, high-throughput screening, and catalyst recycling could accelerate this process. (3) Deeper understanding of the synergistic mechanisms in dual-metal catalysts is needed to guide the rational design of more efficient catalysts. Advanced characterization techniques, such as *operando* spectroscopy and *in situ* electron microscopy, could provide valuable insights. (4) Achieving high selectivity towards multi-carbon products remains a challenge. The optimization of catalyst composition, structure and reaction conditions could pave the way for the efficient production of C_{2+} compounds from the CO_2RR.

In summary, dual-metal catalysis with synergistic effects holds great promise for advancing the field of the CO_2RR. With continued research efforts in catalyst design, synthesis, and mechanistic understanding, the efficient conversion of CO_2 into value-added products could become a reality, contributing significantly to global carbon neutrality goals.

Data availability

No primary research results, software or code have been included and no new data were generated or analysed as part of this review.

Author contributions

M. W. and T. L. conceived the topic and revised the review. M. W., P. S. and Y. Y wrote and edited the original draft of the manuscript. All authors helped in literature search.

Conflicts of interest

The authors declare no conflict of interest.

Acknowledgements

This work was supported by the National Natural Science Foundation of China (22375148) and the National Key R&D Program of China (2022YFA1502902).

Notes and references

1 A. Husile, Z. Wang and J. Guan, *Chem. Sci.*, 2025, **16**, 5413–5446.
2 D. Suri, S. Das, S. Choudhary, G. Venkanna, B. Sharma, M. A. Afroz, N. K. Tailor, R. Joshi, S. Satapathi and K. Tripathi, *Small*, 2025, **21**, 2408981.
3 S. A. Montzka, E. J. Dlugokencky and J. H. Butler, *Nature*, 2011, **476**, 43–50.
4 H. M. A. Sharif, M. Rashad, I. Hussain, A. Abbas, O. F. Aldosari and C. Li, *Appl. Catal. B Environ. Energy*, 2024, **344**, 123585.
5 W. Lai, Z. Ma, J. Zhang, Y. Yuan, Y. Qiao and H. Huang, *Adv. Funct. Mater.*, 2022, **32**, 2111193.
6 M. J. Gidden, T. Gasser, G. Grassi, N. Forsell, I. Janssens, W. F. Lamb, J. Minx, Z. Nicholls, J. Steinhauser and K. Riahi, *Nature*, 2023, **624**, 102–108.
7 B. Buchner, *Science*, 2024, **386**, 601.
8 L. Wang, D. Wang and Y. Li, *Carbon Energy*, 2022, **4**, 1021–1079.
9 W. Peng, F. Li, S. Kong, C. Guo, H. Wu, J. Wang, Y. Shen, X. Meng and M. Zhang, *Carbon Energy*, 2024, **6**, e498.
10 J. Han, X. Bai, X. Xu, X. Bai, A. Husile, S. Zhang, L. Qi and J. Guan, *Chem. Sci.*, 2024, **15**, 7870–7907.
11 Z. Wang, Z. Sun, H. Yin, H. Wei, Z. Peng, Y. X. Pang, G. Jia, H. Zhao, C. H. Pang and Z. Yin, *eScience*, 2023, **3**, 100136.
12 Y. Yang, S. Louisia, S. Yu, J. Jin, I. Roh, C. Chen, M. V. Fonseca Guzman, J. Feijóo, P.-C. Chen, H. Wang, C. J. Pollock, X. Huang, Y.-T. Shao, C. Wang, D. A. Muller, H. D. Abruña and P. Yang, *Nature*, 2023, **614**, 262–269.
13 N. Dutta and S. C. Peter, *J. Am. Chem. Soc.*, 2025, **147**, 9019–9036.
14 G. Liang, S. Yang, C. Wu, Y. Liu, Y. Zhao, L. Huang, S. Zhang, S. Dou, H. Du, D. Cui and L. Lin, *J. Mater. Chem. A*, 2025, **13**, 11210–11235.
15 J. Jia, Z. Zhang, A. Wang, Y. Liu, Z. Liu, J. Wang, Y. Guo, L. Peng, J. Li and J. Robertson, *Adv. Funct. Mater.*, 2025, **35**, 2412056.
16 W. Lai, Y. Qiao, Y. Wang and H. Huang, *Adv. Mater.*, 2023, **35**, 2306288.
17 F. Xie, Z. Wang, C.-W. Kao, J. Lan, Y.-R. Lu and Y. Tan, *Angew. Chem., Int. Ed.*, 2024, **63**, e202407661.
18 B. Lei, W. Cui, P. Chen, L. Chen, J. Li and F. Dong, *ACS Catal.*, 2022, **12**, 9670–9678.
19 J. Xiong, J. Ji, Q. Lei, X. Yang, Y. Bai, X. Zhang and H.-M. Cheng, *eScience*, 2024, 100306.

20 K. Wang, K. Huang, Z. Wang, G. An, M. Zhang, W. Liu, S. Fu, H. Guo, B. Zhang, C. Lian, J. Wu and L. Wang, *Small*, 2025, 2502733.
21 Q. Yang, H. Liu, Y. Lin, D. Su, Y. Tang and L. Chen, *Adv. Mater.*, 2024, **36**, 2310912.
22 H. Zhao, R. Yu, S. Ma, K. Xu, Y. Chen, K. Jiang, Y. Fang, C. Zhu, X. Liu, Y. Tang, L. Wu, Y. Wu, Q. Jiang, P. He, Z. Liu and L. Tan, *Nat. Catal.*, 2022, **5**, 818–831.
23 H. Ou, S. Ning, P. Zhu, S. Chen, A. Han, Q. Kang, Z. Hu, J. Ye, D. Wang and Y. Li, *Angew. Chem., Int. Ed.*, 2022, **61**, e202206579.
24 Z. Wu, N. Meng, R. Yang, M. Chen, J. Pan, S. Chi, C. Wu, S. Xi, Y. Liu, Y. Ou, W. Wu, S. Han, B. Zhang, Q.-H. Yang and K. Ping Loh, *Angew. Chem., Int. Ed.*, 2025, **64**, e202420283.
25 C.-f. Li, R.-t. Guo, Z.-r. Zhang, T. Wu and W.-g. Pan, *Small*, 2023, **19**, 2207875.
26 M. Kuang, B. Li, L. Zhou, Z. Huang, J. Wu, S. Wang and J. Yang, *Angew. Chem., Int. Ed.*, 2025, **64**, e202422357.
27 Y.-F. Tang, L.-B. Liu, M. Yu, S. Liu, P.-F. Sui, W. Sun, X.-Z. Fu, J.-L. Luo and S. Liu, *Chem. Soc. Rev.*, 2024, **53**, 9344–9377.
28 T. Lu, T. Xu, S. Zhu, J. Li, J. Wang, H. Jin, X. Wang, J.-J. Lv, Z.-J. Wang and S. Wang, *Adv. Mater.*, 2023, **35**, 2310433.
29 H. Shang and D. Liu, *Nano Res.*, 2023, **16**, 6477–6506.
30 J. Liu, Y. Cai, R. Song, S. Ding, Z. Lyu, Y.-C. Chang, H. Tian, X. Zhang, D. Du, W. Zhu, Y. Zhou and Y. Lin, *Mater. Today*, 2021, **48**, 95–114.
31 Y. Zhai, P. Han, Q. Yun, Y. Ge, X. Zhang, Y. Chen and H. Zhang, *eScience*, 2022, **2**, 467–485.
32 J. Wang, D. Deng, Q. Wu, M. Liu, Y. Wang, J. Jiang, X. Zheng, H. Zheng, Y. Bai, Y. Chen, X. Xiong and Y. Lei, *ACS Nano*, 2023, **17**, 18688–18705.
33 C. Wang, Z. Lv, X. Feng, W. Yang and B. Wang, *Adv. Energy Mater.*, 2024, **14**, 2400160.
34 J. Huang, T. Yang, K. Zhao, S. Chen, Q. Huang and Y. Han, *J. Energy Chem.*, 2021, **62**, 71–102.
35 P. Sun, S. Liu, X. Zheng, G. Hu, Q. Zhang, X. Liu, G. Zheng and Y. Chen, *Nano Today*, 2024, **55**, 102152.
36 P. Li, J. Liu, Y. Wang, X.-D. Zhang, Y. Hou, Y. Zhang, X. Sun, X. Kang, Q. Zhu and B. Han, *J. Am. Chem. Soc.*, 2024, **146**, 26525–26533.
37 Q. Zhang, D. Liu, Y. Zhang, Z. Guo, M. Chen, Y. Chen, B. Jin, Y. Song and H. Pan, *J. Energy Chem.*, 2023, **87**, 509–517.
38 Y. Li, H. Wang, X. Yang, T. O'Carroll and G. Wu, *Angew. Chem., Int. Ed.*, 2024, **63**, e202317884.
39 L. Shi, J. Song, Y. Yang, L. Yang, Z. Dai, L. Yao and W. Jiang, *J. Mater. Chem. A*, 2025, **13**, 2478–2504.
40 J. Jiao, Q. Yuan, M. Tan, X. Han, M. Gao, C. Zhang, X. Yang, Z. Shi, Y. Ma, H. Xiao, J. Zhang and T. Lu, *Nat. Commun.*, 2023, **14**, 6164.
41 B. Ren, G. Wen, R. Gao, D. Luo, Z. Zhang, W. Qiu, Q. Ma, X. Wang, Y. Cui, L. Ricardez-Sandoval, A. Yu and Z. Chen, *Nat. Commun.*, 2022, **13**, 2486.
42 W. Wu, J. Zhu, Y. Tong, S. Xiang and P. Chen, *Nano Res.*, 2024, **17**, 3684–3692.
43 A. R. Woldu, A. G. Yohannes, Z. Huang, P. Kennepohl, D. Astruc, L. Hu and X.-C. Huang, *Adv. Mater.*, 2024, **36**, 2414169.
44 Y. Gao, B. Liu and D. Wang, *Adv. Mater.*, 2023, **35**, 2209654.
45 Y. Yang, W. Zhang, G. Wu, Q. Huang, J. Wen, D. Wang and M. Liu, *Angew. Chem., Int. Ed.*, 2025, e202504423.
46 Y. Chen, J. Zhao, X. Pan, L. Li, Z. Yu, X. Wang, T. Ma, S. Lin and J. Lin, *Angew. Chem., Int. Ed.*, 2024, **63**, e202411543.
47 J. Feng, L. Zhang, S. Liu, L. Xu, X. Ma, X. Tan, L. Wu, Q. Qian, T. Wu, J. Zhang, X. Sun and B. Han, *Nat. Commun.*, 2023, **14**, 4615.
48 J. Li, Y. Chen, B. Yao, W. Yang, X. Cui, H. Liu, S. Dai, S. Xi, Z. Sun, W. Chen, Y. Qin, J. Wang, Q. He, C. Ling, D. Wang and Z. Zhang, *J. Am. Chem. Soc.*, 2024, **146**, 5693–5701.
49 J. Liu, P. Li, J. Bi, S. Jia, Y. Wang, X. Kang, X. Sun, Q. Zhu and B. Han, *J. Am. Chem. Soc.*, 2023, **145**, 23037–23047.
50 W. Zhu, L. Zhang, S. Liu, A. Li, X. Yuan, C. Hu, G. Zhang, W. Deng, K. Zang, J. Luo, Y. Zhu, M. Gu, Z.-J. Zhao and J. Gong, *Angew. Chem., Int. Ed.*, 2020, **59**, 12664–12668.
51 W. Xu, Y. Wang, C. Zhang, X. Ma, J. Wu, Y. Liu, B. Lu, H. Zhang, C. Ming and J. Xiang, *Chem. Eng. J.*, 2023, **461**, 141911.
52 R. Cao, S. Yin, Y. Han, J. Zhang, W. Jiang and G. Liu, *Coord. Chem. Rev.*, 2025, **538**, 216722.
53 J. Ji, L. Wu, S. Zhou, T. Qiu, Z. Li, L. Wang, L. Zhang, L. Ma, M. Ling, S. Zhou and C. Liang, *Small Methods*, 2022, **6**, 2101511.
54 H. Shang, S. K. Wallentine, D. M. Hofmann, Q. Zhu, C. J. Murphy and L. R. Baker, *Chem. Sci.*, 2020, **11**, 12298–12306.
55 B. Zhao, F. Chen, C. Cheng, L. Li, C. Liu and B. Zhang, *Adv. Energy Mater.*, 2023, **13**, 2204346.
56 M. Jun, J. Kundu, D. H. Kim, M. Kim, D. Kim, K. Lee and S.-I. Choi, *Adv. Mater.*, 2024, **36**, 2313028.
57 Z.-Q. Liang, T.-T. Zhuang, A. Seifitokaldani, J. Li, C.-W. Huang, C.-S. Tan, Y. Li, P. De Luna, C. T. Dinh, Y. Hu, Q. Xiao, P.-L. Hsieh, Y. Wang, F. Li, R. Quintero-Bermudez, Y. Zhou, P. Chen, Y. Pang, S.-C. Lo, L.-J. Chen, H. Tan, Z. Xu and S. Zhao, *Nat. Commun.*, 2018, **9**, 3828.
58 M. Qi, M. J. Zachman, Y. Li, Y. Zeng, S. Hwang, J. Liang, M. Lyons, Q. Zhao, Y. Mao, Y. Shao, Z. Feng, Z. Wang, Y. Zhao and G. Wu, *Energy Environ. Sci.*, 2025, **18**, 5643–5656.
59 S. A. Chala, R. Liu, E. O. Oseghe, S. T. Clausing, C. Kampf, J. Bansmann, A. H. Clark, Y. Zhou, I. Lieberwirth, J. Biskupek, U. Kaiser and C. Streb, *ACS Catal.*, 2024, **14**, 15553–15564.
60 Y. Song, J. R. C. Junqueira, N. Sikdar, D. Öhl, S. Dieckhöfer, T. Quast, S. Seisel, J. Masa, C. Andronescu and W. Schuhmann, *Angew. Chem., Int. Ed.*, 2021, **60**, 9135–9141.
61 Z. Zhang, S. Li, Y. Rao, L. Yang, W. Yan and H. Xu, *Chem. Eng. J.*, 2024, **479**, 147376.
62 M. Li, S. Kuang, Y. Jin, H. Chi, S. Zhang and X. Ma, *Chem. Eng. J.*, 2025, **506**, 160048.

63 M.-G. Kim, J. Park, Y. Choi, H. C. Song, S.-H. Kim, K.-M. Bang, H. C. Ham, N.-K. Kim, D. H. Won, B. K. Min, S. J. Yoo and W. Kim, *Adv. Energy Mater.*, 2023, **13**, 2300749.
64 R. Zhang, H. Ma, S. Han, Z. Wu, X. Zhou, Z. Chen, J. Liu, Y. Xiao, W. Chen and K. P. Loh, *Angew. Chem., Int. Ed.*, 2025, **64**, e202421860.
65 Z. Ren, B. Li, Y. Wu, H. Liu, F. Guo, S. Tian and J. Yang, *Chem. Eng. J.*, 2025, **507**, 160394.
66 L. Yan, W. Su, X. Cao, P. Zhang and Y. Fan, *Chem. Eng. J.*, 2021, **412**, 128718.
67 L. Xue, Q.-Y. Fan, Y. Zhao, Y. Liu, H. Zhang, M. Sun, Y. Wang and S. Zeng, *J. Energy Chem.*, 2023, **82**, 414–422.
68 S. You, J. Xiao, S. Liang, W. Xie, T. Zhang, M. Li, Z. Zhong, Q. Wang and H. He, *Energy Environ. Sci.*, 2024, **17**, 5795–5818.
69 X. Shi, L. Shi, J. Wang, Y. Zhou and S. Zhao, *Matter*, 2024, **7**, 4233–4259.
70 F. Huang, X. Chen, H. Sun, Q. Zeng, J. Ma, D. Wei, J. Zhu, Z. Chen, T. Liang, X. Yin, X. Liu, J. Xu and H. He, *Angew. Chem., Int. Ed.*, 2025, **64**, e202415642.
71 W. Guo, S. Liu, X. Tan, R. Wu, X. Yan, C. Chen, Q. Zhu, L. Zheng, J. Ma, J. Zhang, Y. Huang, X. Sun and B. Han, *Angew. Chem., Int. Ed.*, 2021, **60**, 21979–21987.
72 K. Wang, D. Liu, L. Liu, J. Liu, X. Hu, P. Li, M. Li, A. S. Vasenko, C. Xiao and S. Ding, *eScience*, 2022, **2**, 518–528.
73 C. Peng, X. Zhu, Z. Xu, S. Yan, L. Y. Chang, Z. Wang, J. Zhang, M. Chen, T.-K. Sham, Y. Li and G. Zheng, *Small*, 2022, **18**, 2106433.
74 C. Li, H. Yan, H. Yang, W. Zhou, C. Xie, B. Pan and Q. Zhang, *Sci. China Mater.*, 2025, **68**, 21–38.
75 L. Zhang, J. Feng, S. Liu, X. Tan, L. Wu, S. Jia, L. Xu, X. Ma, X. Song, J. Ma, X. Sun and B. Han, *Adv. Mater.*, 2023, **35**, 2209590.
76 X. Zhang, C. Liu, Y. Zhao, L. Li, Y. Chen, F. Raziq, L. Qiao, S.-X. Guo, C. Wang, G. G. Wallace, A. M. Bond and J. Zhang, *Appl. Catal. B Environ. Energy*, 2021, **291**, 120030.
77 X. K. Lu, B. Lu, H. Li, K. Lim and L. C. Seitz, *ACS Catal.*, 2022, **12**, 6663–6671.
78 H. Zhang, Y. Cao, M. Sun, Y. Liu, Y. Wang, H. Li, R. Zhang, X. Gu and S. Zeng, *Chem. Eng. J.*, 2024, **490**, 151706.
79 K. Huang, R. Li, H. Qi, S. Yang, S. An, C. Lian, Q. Xu, H. Liu and J. Hu, *ACS Catal.*, 2024, **14**, 8889–8898.
80 H. Wu, J. Li, K. Qi, Y. Zhang, E. Petit, W. Wang, V. Flaud, N. Onofrio, B. Rebiere, L. Huang, C. Salameh, L. Lajaunie, P. Miele and D. Voiry, *Nat. Commun.*, 2021, **12**, 7210.
81 A. Bohan, X. Jin, M. Wang, X. Ma, Y. Wang and L. Zhang, *J. Colloid Interface Sci.*, 2024, **654**, 830–839.
82 Y. Zhu, J. Sokolowski, X. Song, Y. He, Y. Mei and G. Wu, *Adv. Energy Mater.*, 2020, **10**, 1902844.
83 N. Sakamoto, K. Sekizawa, S. Shirai, T. Nonaka, T. Arai, S. Sato and T. Morikawa, *Nat. Catal.*, 2024, **7**, 574–584.
84 Z. Sun, C. Li, Z. Wei, F. Zhang, Z. Deng, K. Zhou, Y. Wang, J. Guo, J. Yang, Z. Xiang, P. Ma, H. Zhai, S. Li and W. Chen, *Adv. Mater.*, 2024, **36**, 2404665.
85 X.-Q. Wang, Q. Chen, Y.-J. Zhou, H.-M. Li, J.-W. Fu and M. Liu, *Adv. Sens. Energy Mater.*, 2022, **1**, 100023.
86 Y. Jia, F. Li, K. Fan and L. Sun, *Adv. Powder Mater.*, 2022, **1**, 100012.
87 Y. Chen, Z. Fan, J. Wang, C. Ling, W. Niu, Z. Huang, G. Liu, B. Chen, Z. Lai, X. Liu, B. Li, Y. Zong, L. Gu, J. Wang, X. Wang and H. Zhang, *J. Am. Chem. Soc.*, 2020, **142**, 12760–12766.
88 H. Zhang, C. He, S. Han, Z. Du, L. Wang, Q. Yun, W. Cao, B. Zhang, Y.-H. Tian and Q. Lu, *Chin. Chem. Lett.*, 2022, **33**, 3641–3649.
89 D. Ma, C. Zhi, Y. Zhang, J. Chen, Y. Zhang and J.-W. Shi, *ACS Nano*, 2024, **18**, 21714–21746.
90 Y. Ma, J. Yu, M. Sun, B. Chen, X. Zhou, C. Ye, Z. Guan, W. Guo, G. Wang, S. Lu, D. Xia, Y. Wang, Z. He, L. Zheng, Q. Yun, L. Wang, J. Zhou, P. Lu, J. Yin, Y. Zhao, Z. Luo, L. Zhai, L. Liao, Z. Zhu, R. Ye, Y. Chen, Y. Lu, S. Xi, B. Huang, C.-S. Lee and Z. Fan, *Adv. Mater.*, 2022, **34**, 2110607.
91 C. Peng, J. Ma, G. Luo, S. Yan, J. Zhang, Y. Chen, N. Chen, Z. Wang, W. Wei, T.-K. Sham, Y. Zheng, M. Kuang and G. Zheng, *Angew. Chem., Int. Ed.*, 2024, **63**, e202316907.
92 L. Li, Y. Zhang, X. Luo, I. Masood ul Hasan, K. Wu, B. Nan, Y. Zhang, N. Xu and J. Qiao, *J. Energy Chem.*, 2023, **86**, 569–578.
93 Y. Li, Y. Jin, X. Zong, X. Zhang, G. Li and Y. Xiong, *J. Mater. Chem. A*, 2023, **11**, 11445–11453.
94 K. H. Dinh, L. T. Menisa, H. Warkentin, T. N. Nguyen and C.-T. Dinh, *ACS Catal.*, 2025, **15**, 5731–5759.
95 Q. Tang, Q. Hao, Q. Zhu, J. Wu, K. Huang, K. Liu and J. Lu, *Adv. Energy Mater.*, 2025, **15**, 2403778.
96 J. Chen, M. R. Ahasan, J.-S. Oh, J. A. Tan, S. Hennessey, M. M. Kaid, H. M. El-Kaderi, L. Zhou, K. U. Lao, R. Wang and W.-N. Wang, *J. Mater. Chem. A*, 2024, **12**, 4601–4609.
97 M. Wu, F. Dong, Y. Yang, X. Cui, X. Liu, Y. Zhu, D. Li, S. Omanovic, S. Sun and G. Zhang, *Electrochem. Energy Rev.*, 2024, **7**, 10.
98 J. Hu, M. Zhou, K. Li, A. Yao, Y. Wang, Q. Zhu, Y. Zhou, L. Huang, Y. Pei, Y. Du, S. Jin and M. Zhu, *Small*, 2023, **19**, 2301357.
99 L. Huang, Z. Liu, G. Gao, C. Chen, Y. Xue, J. Zhao, Q. Lei, M. Jin, C. Zhu, Y. Han, J. S. Francisco and X. Lu, *J. Am. Chem. Soc.*, 2023, **145**, 26444–26451.
100 Z. Zhang, G. Wen, D. Luo, B. Ren, Y. Zhu, R. Gao, H. Dou, G. Sun, M. Feng, Z. Bai, A. Yu and Z. Chen, *J. Am. Chem. Soc.*, 2021, **143**, 6855–6864.
101 Y. Lu, H. Li, H. Sun, J. Zhao, Y. Zhang, Y. Wang, C. Zhu, D. Gao, Y. Tuo, J. Zeng, D. Chen and Z. Yan, *ACS Catal.*, 2024, **14**, 14744–14753.
102 H. Yu, W. Zhao, X. Dong, J. Wang, W. Wang, L.-L. Shen, G.-R. Zhang and D. Mei, *Appl. Catal. B Environ. Energy*, 2025, **363**, 124805.
103 Y. Hu, D. Lu, W. Zhou, X. Wang and Y. Li, *J. Mater. Chem. A*, 2023, **11**, 1937–1943.
104 S. Yan, Z. Chen, Y. Chen, C. Peng, X. Ma, X. Lv, Z. Qiu, Y. Yang, Y. Yang, M. Kuang, X. Xu and G. Zheng, *J. Am. Chem. Soc.*, 2023, **145**, 26374–26382.
105 W. Zhu, L. Zhang, P. Yang, X. Chang, H. Dong, A. Li, C. Hu, Z. Huang, Z.-J. Zhao and J. Gong, *Small*, 2018, **14**, 1703314.

106 X. Yao, D. Cui, C. Zhu, J. He, F. Meng, S. Yang, M. Dong, G. Shan, M. Zhang, C. Sun, X. Wang and Z. Su, *ACS Mater. Lett.*, 2024, **6**, 5112–5119.
107 H. Wang, G. Zhan, C. Tang, D. Yang, W. Liu, D. Wang, Y. Wu, H. Wang, K. Liu, J. Li, M. Huang and K. Chen, *ACS Nano*, 2023, **17**, 4790–4799.
108 R. Nankya, Y. Xu, A. Elgazzar, P. Zhu, T.-U. Wi, C. Qiu, Y. Feng, F. Che and H. Wang, *Angew. Chem., Int. Ed.*, 2024, **63**, e202403671.
109 Q. Zhang, J. Peng, S. Jiang, H. Xiong, X. Fu, S. Shang, J. Xu, G. He and P.-C. Chen, *Appl. Catal. B Environ. Energy*, 2025, **371**, 125255.
110 Z. Zhang, Q. Fang, X. Yang, S. Zuo, T. Cheng, Y. Yamauchi and J. Tang, *Adv. Mater.*, 2025, **37**, 2411498.
111 Z. Niu, X. Gao, S. Lou, N. Wen, J. Zhao, Z. Zhang, Z. Ding, R. Yuan, W. Dai and J. Long, *ACS Catal.*, 2023, **13**, 2998–3006.
112 R. Belgamwar, R. Verma, T. Das, S. Chakraborty, P. Sarawade and V. Polshettiwar, *J. Am. Chem. Soc.*, 2023, **145**, 8634–8646.
113 R. Chen, J. Zhao, X. Zhang, Q. Zhao, Y. Li, Y. Cui, M. Zhong, J. Wang, X. Li, Y. Huang and B. Liu, *J. Am. Chem. Soc.*, 2024, **146**, 24368–24376.
114 M. Qi, Y. Ma, C. Zhang, B. Li, X. Yang, Z. Shi, S. Liu, C. An, J. Jiao and T. Lu, *Sci. China Chem.*, 2025, **68**, 1620–1626.
115 E. Landaeta, N. I. Kadosh and Z. D. Schultz, *ACS Catal.*, 2023, **13**, 1638–1648.
116 Y. Hu, D. Lu, W. Zhou, X. Wang and Y. Li, *J. Mater. Chem. A*, 2023, **11**, 1937–1943.
117 X. Dong, S. Li, C. Zhu, J. Mao, G. Wu, G. Li, G. Feng, A. Chen, Y. Wei, X. Liu, J. Wang, Y. Song, W. Chen and W. Wei, *Appl. Catal. B Environ. Energy*, 2023, **336**, 122929.
118 H. Liu, C. Yang, T. Bian, H. Yu, Y. Zhou, Y. Zhang and L. Sun, *Adv. Energy Mater.*, 2025, 2405658.
119 Y. Shao, Q. Yuan and J. Zhou, *Small*, 2023, **19**, 2303446.
120 J. Zhao and S. Lin, *J. Colloid Interface Sci.*, 2025, **680**, 257–264.
121 H. Liu, C. Yang, T. Bian, H. Yu, Y. Zhou and Y. Zhang, *Angew. Chem., Int. Ed.*, 2024, **63**, e202404123.
122 Q. Hao, H.-x. Zhong, J.-z. Wang, K.-h. Liu, J.-m. Yan, Z.-h. Ren, N. Zhou, X. Zhao, H. Zhang, D.-x. Liu, X. Liu, L.-w. Chen, J. Luo and X.-b. Zhang, *Nat. Synth.*, 2022, **1**, 719–728.
123 X. Zhao, K. Zhao, Y. Liu, Y. Su, S. Chen, H. Yu and X. Quan, *ACS Catal.*, 2022, **12**, 11412.
124 L.-M. Cao, H.-H. Huang, J.-W. Wang, D.-C. Zhong and T.-B. Lu, *Green Chem.*, 2018, **20**, 798–803.
125 Y.-N. Gong, C.-Y. Cao, W.-J. Shi, J.-H. Zhang, J.-H. Deng, T.-B. Lu and D.-C. Zhong, *Angew. Chem., Int. Ed.*, 2022, **61**, e202215187.
126 X.-M. Liang, H.-J. Wang, C. Zhang, D.-C. Zhong and T.-B. Lu, *Appl. Catal. B Environ. Energy*, 2023, **322**, 122073.
127 Z.-W. Chen, H.-J. Wang, C. Liu, X.-L. Lu and T.-B. Lu, *Sci. China Chem.*, 2025, **68**, 570–579.
128 Y. Wang, B. J. Park, V. K. Paidi, R. Huang, Y. Lee, K.-J. Noh, K.-S. Lee and J. W. Han, *ACS Energy Lett.*, 2022, **7**, 640–649.
129 S. Chen, X. Zheng, P. Zhu, Y. Li, Z. Zhuang, H. Wu, J. Zhu, C. Xiao, M. Chen, P. Wang, D. Wang and Y.-L. He, *Angew. Chem., Int. Ed.*, 2024, **63**, e202411591.
130 G. Yasin, A. Kumar, S. Ajmal, M. Asim Mushtaq, M. Tabish, A. Saad, M. A. Assiri, M. Tariq Nazir and Q. Zhuo, *Coord. Chem. Rev.*, 2024, **501**, 215589.
131 L. Zhang, J. Feng, L. Wu, X. Ma, X. Song, S. Jia, X. Tan, X. Jin, Q. Zhu, X. Kang, J. Ma, Q. Qian, L. Zheng, X. Sun and B. Han, *J. Am. Chem. Soc.*, 2023, **145**, 21945–21954.
132 J.-d. Yi, X. Gao, H. Zhou, W. Chen and Y. Wu, *Angew. Chem., Int. Ed.*, 2022, **61**, e202212329.
133 Z. Guo, H. Zhu, G. Yang, A. Wu, Q. Chen, Z. Yan, K. Loon Fow, H. Do, J. D. Hirst, T. Wu and M. Xu, *Chem. Eng. J.*, 2023, **476**, 146556.
134 W. Xie, H. Li, G. Cui, J. Li, Y. Song, S. Li, X. Zhang, J. Y. Lee, M. Shao and M. Wei, *Angew. Chem., Int. Ed.*, 2021, **60**, 7382–7388.
135 H. Zhang, X. Wang, Y. Sun, X. Wang, Z. Tang, S. Li, X. Gao, J. Wang, Z. Hou, K. Nie, J. Xie, Z. Yang and Y.-M. Yan, *Appl. Catal. B Environ. Energy*, 2024, **351**, 123992.
136 T. Zhang, B. Yuan, W. Wang, J. He and X. Xiang, *Angew. Chem., Int. Ed.*, 2023, **62**, e202302096.
137 L. Yin, Z. Li, J. Feng, P. Zhou, L. Qiao, D. Liu, Z. Yi, W. F. Ip, G. Luo and H. Pan, *ACS Appl. Mater. Interfaces*, 2023, **15**, 47135–47144.
138 M. Wang, H. Chen, M. Wang, J. Wang, Y. Tuo, W. Li, S. Zhou, L. Kong, G. Liu, L. Jiang and G. Wang, *Angew. Chem., Int. Ed.*, 2023, **62**, e202306456.
139 Y. Cao, S. Chen, S. Bo, W. Fan, J. Li, C. Jia, Z. Zhou, Q. Liu, L. Zheng and F. Zhang, *Angew. Chem., Int. Ed.*, 2023, **62**, e202303048.
140 L. Chen, J. Chen, W. Fu, J. Chen, D. Wang, Y. Xiao, S. Xi, Y. Ji and L. Wang, *Nat. Commun.*, 2024, **15**, 7053.
141 A. Saxena, S. Kapila, J. E. Medvedeva and M. Nath, *ACS Appl. Mater. Interfaces*, 2023, **15**, 14433–14446.
142 F. Chang, K. Zhu, C. Liu, J. Wei, S. Yang, Q. Zhang, L. Yang, X. Wang and Z. Bai, *Adv. Funct. Mater.*, 2024, **34**, 2400893.
143 R. Yun, F. Zhan, X. Wang, B. Zhang, T. Sheng, Z. Xin, J. Mao, S. Liu and B. Zheng, *Small*, 2021, **17**, 2006951.
144 Y. Jiang, C. Lv, B. Lu, Y. Song, T. Liu, X. Zhang, D. Gao, K. Ye and G. Wang, *ACS Nano*, 2025, **19**, 11263–11272.
145 S. Shen, X. Peng, L. Song, Y. Qiu, C. Li, L. Zhuo, J. He, J. Ren, X. Liu and J. Luo, *Small*, 2019, **15**, 1902229.
146 P. Luan, X. Dong, L. Liu, J. Xiao, P. Zhang, J. Zhang, H. Chi, Q. Wang, C. Ding, R. Li and C. Li, *ACS Catal.*, 2024, **14**, 8776–8785.
147 M. Chhetri, M. Wan, Z. Jin, J. Yeager, C. Sandor, C. Rapp, H. Wang, S. Lee, C. J. Bodenschatz, M. J. Zachman, F. Che and M. Yang, *Nat. Commun.*, 2023, **14**, 3075.
148 Y. Zheng, J. Zhang, Z. Ma, G. Zhang, H. Zhang, X. Fu, Y. Ma, F. Liu, M. Liu and H. Huang, *Small*, 2022, **18**, 2201695.
149 X. Li, M. Qin, X. Wu, X. Lv, J. Wang, Y. Wang and H. B. Wu, *Small*, 2023, **19**, 2302530.
150 Z. Wei, S. Yue, S. Gao, M. Cao and R. Cao, *Nano Res.*, 2023, **16**, 7777–7783.
151 T. Wan, C. Lv, K. Ye, M. Ma, D. Hu, J. Xiao and W. Xiao, *Small Methods*, 2025, 2500005.

152 X. Liu, T. Liu, T. Ouyang, J. Deng and Z.-Q. Liu, *Angew. Chem., Int. Ed.*, 2025, **64**, e202419796.
153 H. Zhang, X. Wang, Y. Sun, X. Wang, Z. Tang, S. Li, X. Gao, J. Wang, Z. Hou, K. Nie, J. Xie, Z. Yang and Y.-M. Yan, *Appl. Catal. B Environ. Energy*, 2024, **351**, 123992.
154 Y. Xiao, F. Yu, C. Xia, D. Zhu, J. Chen, N. Liu, Y. Zhao, R. Qi, W. Guo, B. You, T. Yao, Y. Pang, Z. Wang, H. Wang, F. Song and B. Y. Xia, *J. Am. Chem. Soc.*, 2025, **147**, 15654–15665.
155 Z. Guo, H. Zhu, Z. Yan, L. Lei, D. Wang, Z. Xi, Y. Lian, J. Yu, K. L. Fow, H. Do, J. D. Hirst, T. Wu and M. Xu, *Appl. Catal. B Environ. Energy*, 2025, **364**, 124839.
156 Z. Yang, D. Ji, Z. Li, Z. He, Y. Hu, J. Yin, Y. Hou, P. Xi and C.-H. Yan, *Small*, 2023, **19**, 2303099.
157 J. Feng, L. Wu, S. Liu, L. Xu, X. Song, L. Zhang, Q. Zhu, X. Kang, X. Sun and B. Han, *J. Am. Chem. Soc.*, 2023, **145**, 9857–9866.
158 H. Wang, H. Zhang, Y. Huang, H. Wang, A. Ozden, K. Yao, H. Li, Q. Guo, Y. Liu, A. Vomiero, Y. Wang, Z. Qian, J. Li, Z. Wang, X. Sun and H. Liang, *ACS Nano*, 2023, **17**, 346–354.
159 J. Liu, P. Li, S. Jia, Y. Wang, L. Jing, Z. Liu, J. Zhang, Q. Qian, X. Kang, X. Sun, Q. Zhu and B. Han, *Nat. Synth.*, 2025, DOI: **10.1038/s44160-025-00752-4**.
160 J. Feng, L. Wu, X. Song, L. Zhang, S. Jia, X. Ma, X. Tan, X. Kang, Q. Zhu, X. Sun and B. Han, *Nat. Commun.*, 2024, **15**, 4821.
161 X. Zhou, j. Shan, L. Chen, B. Y. Xia, T. Ling, J. Duan, Y. Jiao, Y. Zheng and S. Qiao, *J. Am. Chem. Soc.*, 2022, **144**, 2079–2084.